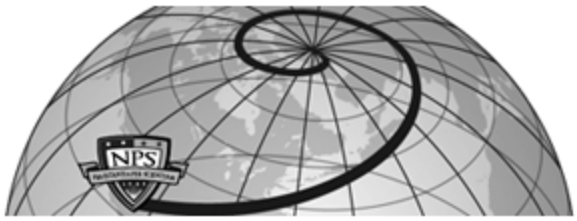

AN EXPERIMENTAL DETERMINATION OF HEAT TRANSFER AND FLOW FRICTION CHARACTERISTICS OF PERFORATED MATERIAL FOR COMPACT HEAT EXCHANGER SURFACES

JOHN M. BANNON

AN EXPERIMENTAL DETERMINATION OF HEAT TRANSFER AND FLOW FRICTION CHARACTERISTICS OF PERFORATED MATERIAL FOR COMPACT HEAT EXCHANGER SURFACES

* * * * *

John M. Bannon

AN EXPERIMENTAL DETERMINATION OF HEAT TRANSFER AND FLOW FRICTION CHARACTERISTICS OF PERFORATED MATERIAL FOR COMPACT HEAT EXCHANGER SURFACES

by

John M. Bannon

Lieutenant, United States Navy

Submitted in partial fulfillment of
the requirements for the degree of

MASTER OF SCIENCE
IN
MECHANICAL ENGINEERING

United States Naval Postgraduate School
Monterey, California

1 9 6 4

AN EXPERIMENTAL DETERMINATION OF HEAT TRANSFER AND FLOW FRICTION CHARACTERISTICS OF PERFORATED MATERIAL FOR COMPACT HEAT EXCHANGER SURFACES

by

John M. Bannon

This work is accepted as fulfilling

the thesis requirements for the degree of

MASTER OF SCIENCE

IN

MECHANICAL ENGINEERING

from the

United States Naval Postgraduate School

ABSTRACT

The transient testing technique for the determination of heat transfer characteristics of a porous medium has been known since 1929. It requires a good deal of care and one of the important restrictions is a step change in temperature must be applied to the medium at the beginning of a test run. This thesis involves the design, test and evaluation of an experimental set-up that utilizes an "integral heater" to accomplish the step change in temperature. In addition, there is presented heat transfer and flow friction characteristics for a 20° skew matrix constructed from perforated nickel material. This data is compared to a 20° skew matrix made from stainless steel material that has been previously reported by C. P. Howard. Also, data is presented for two "parallel plate" matrices, one constructed from brass sheet, the other from perforated nickel material. A comparison of their relative performances is made.

TABLE OF CONTENTS

LIST OF ILLUSTRATIONS

List of Illustrations

LIST OF TABLES

NOMENCLATURE

A = Matrix heat transfer area, ft^2

A_c = Flow cross-section area, ft^2

A_{fr} = Matrix frontal area, ft^2

A_s = Solid matrix cross-section area available for thermal conduction, ft^2

$\overline{A}_s$ = Conduction area corrected for effect of slots ft^2

c_p = Specific heat of fluid at constant pressure, BTU/lb°F

c_s = Matrix material specific heat, BTU/lb°F

C = Fluid heat capacitance, mc_p, BTU/°F sec

$\overline{C}_s$ = Matrix heat capacitance, $W_s c_s$, BTU/°F

D_H = Hydraulic Diameter, $4r_H$, ft

E = Flow friction power per unit area, hp/ft^2

G = Mass flow velocity, $lb/hr\ ft^2$

g_c = Proportionality constant, 32.20 ft lb/# sec^2

h = Unit conductance for convective heat transfer or heat transfer power per unit area per degree temperature difference, BTU/hr °F ft^2

k = Fluid thermal conductivity, BTU/hr°F ft

k_s = Matrix material thermal conductivity, BTU/hr°F ft

L = Matrix Flow length, ft

$\dot{m}$ = Mass flow rate, lb/hr

P = pressure, lb/hr

r_H = Hydraulic radius, ft

V_m = Matrix Volume ft^3

$\overline{V}_s$ = Material volume corrected for effect of slots

V_s = Material volume ft^3

W_s = Matrix mass, lb

β = Matrix compactness, ft^2/ft^3

$\bar{\beta}$ = Compactness corrected for effect of slots

μ = Fluid viscosity, lb/hr ft

γ = Heat transfer area reduction factor

δ = Conduction area reduction factor

ρ = Fluid density, lb/ft^3

ρ_s = Matrix density, lb/ft^3

Nondimensional parameters:

f = Fanning friction factor, ratio of the wall shear stress to the fluid dynamic head

j = Colburn j factor, $N_{ST}N_{PR}^{2/3}$

N_{NU} = Nusselt's number, $\frac{h D_H}{k}$,

N_R = Reynold's number $4r_H G/$

N_{ST} = Stanton number, h/Gc_p

N_{PR} = Prandtl number, $\mu c_p/k$

N_{tu} = Number of heat transfer units, $hA/\dot{m}c_p$

K_e = Entrance flow coefficient for the matrix

K_c = Exit flow coefficient for the matrix

p = porosity of the matrix
Matrix flow void volume/Matrix volume

λ = Conduction parameter, $k_s A_s/L\dot{m}c_p$

Subscripts:

i = initial

1 = upstream

2 = downstream

f = fluid

s = solid (matrix material)

STD = Standard temperature and pressure

1. INTRODUCTION.

A compact heat exchanger is one not necessarily of small bulk and weight, but one which incorporates a heat transfer surface having a high area density.

Arbitrarily, it has been specified that $\beta \geq 200\ ft^2/ft^3$ makes for a compact heat exchanger, where β is the ratio of the heat transfer area to core volume, ft^2/ft^3. (15)+

Motivation for using compact surfaces is to gain high exchanger effectiveness in given box volume and weight limitations and at a reasonable cost. Great impetus has been given the compact heat exchanger field by recent applications as a regenerator in aircraft turboprop power plants, as a regenerator in the gas turbine automobile engine and by their use in cryogenic plant exchangers in the production of liquid oxygen and nitrogen. As the applications for compact heat exchangers increase, design problems increase. A successful compact heat exchanger design and development program requires access to, or the ability to generate knowledge of the basic heat transfer and friction behavior of compact surfaces of interest. It is also desirable that the designer would have available as much information on surface performances as possible to remain flexible in his design with regard to the limitations that have been placed upon him.

Building a complete heat exchanger to evaluate a new surface as to its heat transfer and friction performance would be prohibitively expensive. The alternate method is to generate the performance characteristics of a surface of interest by testing small matrix modules and use

+Numbers in parentheses refer to references in the bibliography.

this data to design a prototype heat exchanger.

Briefly, the objectives of this thesis are: to build an experimental rig that will test small matrix modules to determine their heat transfer and flow friction characteristics, and, to test matrices made from perforated nickel material to determine these characteristics.

One of the simplest and most satisfactory methods of measuring the forced convection heat transfer characteristics of a matrix utilizes a transient test technique or so called single blow method. This test technique consists of heating the homogeneous porous solid of known weight and geometry with a uniformly distributed heat source and then at a given instant, removing the heat source and simultaneously cooling the solid with a fluid at a uniform lower temperature. The heating and cooling steps can be reversed and the same results achieved. A time-temperature response curve of the fluid stream leaving the solid is recorded. By comparing this record to theoretically developed non-dimensional temperature response curves, the heat transfer characteristics of the solid can be determined.

2. SUMMARY OF THEORY.

A theoretical analysis of the transient heat transfer behavior of a porous medium was presented by Schumann (2) in 1929. A porous medium may be defined as an aggregation of solid bodies so arranged that the void spaces between the bodies are connected and will permit the passage of a fluid. This definition can of course be extended to include the matrix surfaces utilized in a compact heat exchanger.

In Schumann's analysis, the porous medium is considered to be homogeneous and initially at a uniform temperature, t_i. A fluid at the same temperature is flowing through the medium. At a certain instant the temperature of the entering fluid is assumed to change to a higher temperature t_{f1}. The problem is then to find the temperature of the fluid and the solid as functions of time and position in the matrix or porous media. The basis of the analysis are the theoretical generalized heating curves that are developed from an energy balance on the matrix.

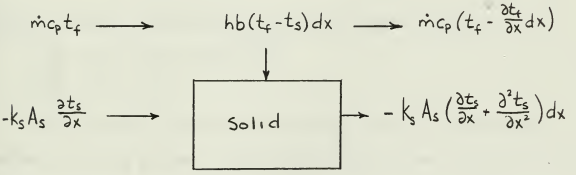

Assume:

1) Properties of the fluid are independent of temperature.
2) Fluid flow is steady.
3) The porous solid is homogeneous.
4) The thermal conductivity of both fluid and solid is infinite perpendicular to the flow direction.
5) Thermal conductivity of fluid is zero in the flow direction.

Heat absorbed by the solid = $\rho_s A_s c_s \frac{\partial t_s}{\partial \theta} dx$

Heat transferred to solid by convection = $hb(t_f - t_s)dx$

Heat transferred from the fluid by convection = $\dot{m} c_p \frac{\partial t_f}{\partial x} dx$

Heat transferred from solid by conduction = $- k_s A_s \frac{\partial^2 t_s}{\partial x^2} dx$

An energy balance for the fluid and solid results in:

$$\rho_s A_s c_s \frac{\partial t_s}{\partial \theta} dx = k_s A_s \frac{\partial^2 t_s}{\partial x^2} dx + hb(t_f - t_s) dx \qquad (1)$$

$$\dot{m} c_p \frac{\partial t_f}{\partial x} dx + hb(t_f - t_s) dx = 0 \qquad (2)$$

Let: τ = generalized time variable = $\frac{hA}{W_s c_s} \theta$

z = generalized position variable = $N_{tu} \frac{x}{L}$

$$N_{tu} = \frac{h}{\dot{m}} \frac{A}{c_p} \qquad \lambda = \frac{k_s}{\dot{m}} \frac{A_s}{c_p L}$$

Making the above substitutions, equations 1) and 2) become:

$$\frac{\partial t_s}{\partial \tau} = (t_f - t_s) + \lambda N_{tu} \frac{\partial^2 t_s}{\partial z^2}$$

$$\frac{\partial t_f}{\partial z} = (t_s - t_f)$$

The experimental method used requires that the above assumptions and the following boundary and initial conditions be closely observed. These conditions are as follows:

1) Initially the core is at a uniform temperature.

2) At time t = 0, the temperature of the incoming fluid changes instantaneously.

3) System is adiabatic, that is, only heat is transferred between the matrix core and the fluid, none with the surroundings.

With the idealizations, initial and boundary conditions, and the additional assumption that the thermal conduction in the solid is zero parallel to the direction of fluid flow (i.e., λ , the material conduction parameter, = 0), Schumann's solutions are as follows:

$$\frac{t_f - t_i}{t_{fl} - t_i} = 1 - e^{-(z + \tau)} \sum_{n=1}^{\infty} z^n \frac{d^n}{d(z\tau)^n} J_o (2i\sqrt{\tau z}) \ldots.$$

$$\frac{t_s - t_i}{t_{fl} - t_i} = 1 - e^{-(z + \tau)} \sum_{n=0}^{\infty} z^n \frac{d^n}{d(z\tau)^n} J_o (2i\sqrt{\tau z})$$

This solution was first used as the basis for a transient technique by Furnas (16) in 1932. The fluid temperature was measured at the exit of the matrix where x = L, therefore z = N_{tu}. The experimental data was compared with Schumann's theoretical constant z curves. The theoretical z curve which best fit the experimental data was considered as the N_{tu} of the matrix and from this value, h, the convection conductance was determined. The biggest disadvantage of this method is in the calculation of an infinite series for each point and the number of terms necessary for a good approximation increases as N_{tu} increases.

In 1950, G. L. Locke (1) developed another method for the evaluation of experimental N_{tu} from the theoretical curves. In this method, only the maximum slopes of the theoretical and experimental curves need to be compared. He derived an expression for the slope of the generalized heating curve, $(t_f - t_i)/(t_{fl} - t_i)$ vs. τ/z, as a function of N_{tu}. Locke's

expression shows that the maximum slope of the generalized heating curve is a unique function of N_{tu}:

$$\frac{d\left(\frac{t_{f2} - t_i}{t_{f1} - t_i}\right)}{d(\tau / N_{tu})} = \frac{N_{tu}^2}{\sqrt{N_{tu}\,\tau}} \left[- J_1\left(2i\sqrt{\tau N_{tu}}\right) e^{-(N_{tu} + \tau)} \right]$$

The above implies that the downstream fluid temperature is measured at $x = L$. Therefore, $z = N_{tu}$ and $t_f = t_{f2}$. This method has become known as "The Maximum Slope Method".

One of the idealizations made by Schumann and followed by Locke was that the thermal conductivity of the solid parallel to the flow is zero. This is very difficult to achieve in an experiment with a continuous flow channel in the matrix. Although the effect of finite thermal conductivity parallel to the flow is negligible at high Reynold's numbers, it cannot be ignored at low Reynold's numbers. Recent works by Crestwick (3), Mondt (4), and Howard (5) consider the effects of longitudinal thermal conduction in the solution of Schumann's transient heating problem. To correlate results, they utilize the conduction parameter, λ. This parameter is the ratio of conduction heat transfer to the change in internal thermal energy of the flowing fluid for the same temperature difference. When $\lambda = 0$, the maximum slope is a unique function of N_{tu}, as put forth by Locke, however, when $\lambda \neq 0$, the maximum slope is a function of N_{tu} and λ.

Howard, in his paper (5), included graphs and a table of maximum slopes as a function of N_{tu} and λ. He derived these values by finite difference calculations on a digital computer and proposed that the values of maximum slopes, as presented, are within $\pm$ 2% for a given N_{tu} and λ.

Ideally then, if the idealizations, initial and boundary conditions can be adhered to, all that is required for the experimental evaluation of the heat transfer characteristics of a matrix is to:

1) Determine the conduction parameter λ .
2) Experimentally determine the maximum slope of the heating or cooling curve.

3. OBJECTIVES.

In the past, there has been a variety of experiments conceived to utilize the principles previously discussed, by approaching the idealizations, initial and boundary conditions as closely as possible. Perhaps the most difficult condition to achieve is; "at time t = 0 the temperature of the incoming fluid changes instantaneously".

Locke (1) and Coppage (9) both employed an air switching device with which air could be quickly directed through the matrix or by-passed to the atmosphere. By use of this switch they imposed a "step change" in temperature on their test matrices. To approach the "step change" in temperature, "requires a fast operating fluid switch for introducing the hotter (or colder) fluid in order to assure an instantaneous change of fluid temperature. However, even with rapid switching, one of the major difficulties here is the inevitable thermal capacity of ducting, switch device and matrix holding device causes unavoidable changes in the entering temperature". (9)

Solar Aircraft Company recently did some work testing core modules for their T-600 engine (10). In their experimental rig, they utilized two steady streams of air and a carriage tray that houses the core module. The tray was inserted through the side of the test cabinet and was moved from a warm air stream to a ambient or cold air stream to simulate a step flunction change of temperature. This type of switching was done manually.

Howard, in his work with new compact surfaces (6), employed a "sliding drawer". This drawer holds the matrix and the downstream thermocouples. The drawer can be inserted or withdrawn from the test section

through which ambient air flows continuously. The matrix is heated when the drawer is in the withdrawn position by an independent temperature controlled air stream.

One of the objectives of this thesis was to construct and test an experimental rig that would improve upon those previously used. This test apparatus described herein differs from other test facilities chiefly in the method used to simulate the initial condition of a step change in temperature of the fluid (air).

The test apparatus constructed has but one air stream, the air is heated by a high resistance nichrome wire heater complex, an integral part of the apparatus, located just upstream of the test matrix. The time constant or response of the heaters is at least an order of magnitude smaller than the response of the thermocouples and recording devices used. By turning the heaters on or off, the step change in temperature is simulated. The other systems required some manual dexterity on the part of the experimenter to begin a data run, whereas this system involves only turning off or on the heaters. The temperature recording device is started prior to the start of a run. The results achieved by this system were an improvement over other systems. With the "sliding drawer" and "quick changing valve" there is a change in the flow and therefore the hydrodynamic as well as the thermal boundary layer must develope. In this system, the hydrodynamic boundary layer is already formed, only the thermal boundary layer is affected. A complete description of equipment is presented in APPENDIX B.

In addition to the construction of this test apparatus and the verification of its reliability by comparing with published data, extension of the curves published by Howard (6) into the high Reynold's number region was attempted.

Finally, heat transfer and flow friction characteristics of several new surfaces were determined.

4. EXPERIMENTAL TECHNIQUES

In reference (5) Howard presents results from a numerical finite-difference method of calculating the transient behavior of a porous media when subjected to a step change in fluid temperature. These calculations consider the case where longitudinal thermal heat conduction cannot be neglected. These data are intimately involved in the determination of N_{tu} and subsequently the Colburn j factor as presented in this thesis. For this reason the restrictions, idealizations and conditions Howard placed on his solution will be restated here. It is these restrictions, idealizations and conditions that the experimental set-up must approach as closely as possible to achieve reliable results.

1) The flow entering the matrix is steady and uniform in velocity and temperature, and remains steady and uniform at any cross section as it flows through the matrix.

2) The thermal conductivity of the matrix is infinite in the direction normal to the flow and finite in the direction parallel to the flow.

3) The thermal capacity of the fluid contained at any time within the matrix is small compared with the thermal capacity of the matrix.

4) The thermal properties of the fluid and matrix are constant and uniform.

5) The convective heat transfer coefficient is some suitable average and remains uniform and constant.

6) At time zero the change in fluid temperature will be a step function, with the matrix and its entrained fluid initially at some uniform and equal temperature.

The first idealization was attained by careful experimentation. Uniform velocity profiles were obtained by wire screen flow straighteners. Uniform temperature profiles were obtained by a wire screen type heater explained in detail in APPENDIX B. The velocity profiles were taken at the inlet of the matrix over entire range of flow rates to ensure that

the profiles were uniform. The temperature profiles were taken over the entire range of flow rates and found to be uniform within $\pm$ .5°F.

The second idealization cannot be strictly realized in practice. The effect of the deviations from this idealization can be made negligible in the solid if the resistance to heat transfer within the solid is small compared to the heat transfer resistance between the solid and fluid.

The third idealization restricts the fluid to a gas rather than a liquid.

The fourth idealization can be realized if the temperature variation is limited to 20 - 25°F. rise above ambient. This would place the operating temperature range at 60 to 80°F. In this range the thermal properties of the fluid, particularly a gas, vary insignificantly and can be considered, as a good approximation, constant and uniform.

The fifth idealization is imposed upon the computer solution and, of course, the determination of the convective heat transfer coefficient is the ultimate result of the experimental process.

Finally, two sets of thermocouples were placed one upstream and one downstream of the matrix. Prior to the beginning of each run, these thermocouple complexes were read. When a steady temperature differential was indicated, the run was begun.

Herein lies the improvement over the "sliding drawer" technique. A series of nichrome wire heaters were installed in the air stream to heat the air and subsequently the matrix. To begin a run, the heaters were turned on or off, and the temperature vs. time recorder started. The time constant (TC) of the nichrome wire heater is very small (TC = .0425 sec for m = 1000 lb/hr, TC = .259 sec for m = 10 lb/hr) and hence the approach

to the final idealization: at time t = 0 the change in fluid temperature will be a step function.

A schematic diagram of the experimental system in which air is used as the working fluid is shown in Figure 1. Figure 2 is a photograph of the entire test apparatus. Essentially, the system consists of a source of air, an air metering device, flow straightener screen pack, an air heater section, a test matrix, a pressure measuring system and a temperature measuring system.

Air is drawn through the apparatus by a six-stage centrifugal air compressor. Air flow rates are measured by an ASME standard D and D/2 orifice meter with changeable orifice plates. Mass flow through the system is controlled by two sliding valves, one on the inlet to the compressor and one on the compressor outlet. In addition, there is a fine control by-pass valve located just ahead of the compressor. As the air passes through the orifice plate it comes to the screen flow straightener at which point the flow cross-section changes from round to square. The air then flows through the air heater section which serves a dual purpose of straightening the air velocity profile and heating the air. In this section the air is heated uniformly to a predetermined temperature, usually 20°F above ambient. The heated air passes into the matrix and heats the matrix to the same uniform temperature. At this point, a run is ready to start. By referencing the thermocouples downstream of the matrix to the thermocouples upstream of the heaters, the initial temperature differential can be very closely controlled. This temperature differential is continuously recorded by a Leeds and Northrup "Speedomax" strip chart recorder when a run is started. The recorded trace has a distinct advantage in that there is no transposition of data necessary, hence, a decrease in the uncertainty of the results. The resultant trace or curve

is the primary data for determining j. The N_{tu} of the matrix can be evaluated by determining the maximum slope of this fluid temperature difference curve during the cooling transient. This is the basis of the maximum slope technique as developed by Locke (1).

The flow friction performances of the matrices tested were obtained by determining the isothermal pressure drop across the matrix and the mass flow rate of the fluid through the matrix. The pressure drop data were obtained from static pressure taps located in the test section immediately upstream and downstream of the test section. The entering fluid static pressure was also recorded. The mass flow rate data were obtained in the air metering section as previously described. In summary, the following data were recorded for each run:

a) Orifice diameter (D_o)
b) Pressure drop across the orifice (ΔP_o)
c) Pressure drop across the matrix (ΔP_m)
d) Entering static pressure (Ps)
e) Orifice temperature (T_o)
f) Atmosphere pressure (P_a)
g) Temperature-Time cooling or heating curve
h) Temperature recorder chart speed

A complete description of the experimental apparatus and equipment is in APPENDIX B. APPENDIX A discusses the relation of the data to the equations governing j & f.

5. DESCRIPTION OF SURFACES.

There are data presented in this thesis for seven surfaces. Of the seven, three are new. Three of the remaining four surfaces were tested by Howard (6). The remaining surface was used primarily as a test surface to check the reliability of the experimental apparatus.

The test surface was a matrix consisting of 20 randomly stacked stainless steel, 60 x 60 mesh screens. A photograph of the matrix along with a tabulation of its physical and geometrical properties may be found in Figure 3. The heat transfer and flow friction characteristics for such a matrix were published by Coppage in 1952 (9), and was considered a good check on the performance of the experimental set-up.

The three matrices examined by Howard and re-examined in this thesis were:

1) Plate-fin reference matrix
2) 10° skew passage matrix
3) 20° skew passage matrix

These particular surfaces were chosen to provide an additional check on the reliability of the experimental setup and to provide a comparison between the "integral heater" and "sliding drawer" experimental techniques.

The plate-fin surface is formed by corrugated sheets separated by a flat spacing sheet to prevent meshing of the corrugations. This matrix was to serve as a reference, since the theoretical laminar flow solutions for both heat transfer and frictional behavior of triangular cross-sections are available. However, difficulty was encountered in forming the material into triangular cross-sections, and therefore it fails as a reference, but the results were interesting and will be discussed later.

Figure 4 presents photographs of the plate-fin matrix and a tabulation of its' physical and geometrical properties.

The skewed passage also employs corrugated sheets, but unlike the plate-fin, the spacer plate is not included. To prevent meshing of the corrugations, the sheets are skewed relative to one another forming what is defined as the "skew angle". A photograph of the matrix and a tabulation of its properties may be found in Figure 5.

Of the three new surfaces tested, one is a version of the previously tested 20° skew matrix using perforated or slotted nickel plates for a material vice a continuous material. The plates were corrugated on the same device used for the original 20° skew to maintain the same corrugation geometry. The perforations should reduce stagnant areas in the matrix, thereby increasing the heat transfer characteristics.

Finally, two matrices of a parallel plate design were constructed and tested. The "parallel plate" matrix is similar to the plate-fin in that a spacer plate is placed between the formed sheets to prevent meshing. The sheets are formed by rolling. When assembled, the matrix is a maze of rectangular passages with an aspect ratio of 77. Aspect ratio is defined in reference (8) as the ratio of the two sides of a rectnagular flow passage, b/a. The sketch below is, ideally, what was intended in designing the "parallel plate" matrix.

One matrix was formed from a brass material and is used as a reference to theoretical laminar flow data for parallel configurations (8). The second matrix was formed from the perforated nickel plate to examine the effects of the perforations on this type of geometry. Pictures and a tabulation of properties for the "parallel plate" matrices are in Figure 6.

6. PRESENTATION OF RESULTS.

The heat transfer and flow friction data for each matrix are presented in Tables I to VII. These data are also presented in graphic form, the Colburn heat transfer factor, j (= $N_{ST}N_{PR}^{2/3}$), and the friction factor, f, are plotted as functions of Reynold's Number, N_R, in Figures 7 through 16. Plotted also in Figures 13 through 15, for comparison purposes, are the theoretical laminar flow solutions for parallel plates.

For the heat transfer data, Prandtl number (N_{PR}) was not really a test variable, since the working fluid was air at moderate temperatures. $N_{PR}^{2/3}$ is included as an approximation to the effect of Prandtl number over a moderate range of Prandtl numbers. Basic laminar boundary layer solutions indicate that in the Prandtl number range of 0.5 to 1.0 (gases), the Prandtl number enters the solution as approximately the 2/3 power.

Since a moderate temperature range is used in the experiment, air properties throughout the matrix are practically constant. Therefore, all the properties of air used in the calculations of the heat transfer and friction characteristics were those of air at the bulk temperature of the air stream as measured at the orifice inlet.

The Reynold's number is based on the hydraulic diameter and mass flow velocity.

$$N_R = \frac{D_H G}{\mu}$$

The hydraulic diameter is defined as:

$$D_H = 4r_H = 4\left(\frac{\text{Flow Passage Cross-sectional area}}{\text{Flow Passage Wetted Perimeter}}\right)$$

$$= 4 \frac{\text{Void Volume}}{L} \times \frac{L}{\text{Heat Transfer Area}}$$

$$= 4 \frac{A_c}{A} L$$

The mass flow velocity is based on the matrix free flow cross-sectional area:

$$G = \frac{\dot{m}}{A_c} = \frac{\dot{m}}{pA_{fr}}$$

The friction factor includes the entrance, exit and flow acceleration effects. The entrance and exit effects normally provide only a small contribution to the overall pressure drop in a matrix. Core friction is the term that controls the magnitude of the pressure drop. As a result, high accuracy in the evaluation of the entrance and exit loss coefficients is not required. These coefficients k_c and k_e are functions of flow geometry and Reynold's number and were obtained from Chapter IV, Figures 18 to 21, as appropriate, reference (8).

7. UNCERTAINTIES AND LIMITATIONS.

As put forth in the theory, the experimental method utilized, requires great care to approach the idealizations and initial and boundary conditions of the theoretical analysis. The magnitude of errors introduced if the experimental system does not duplicate the ideal system is difficult to evaluate. Each of the conditions and idealizations were carefully considered and the experimental system was designed to approach as closely as possible the ideal system. These items are discussed in the "Experimental Technique" section. No attempt will be made here to evaluate or estimate this type of error.

Other experimental errors are caused by: 1) uncertainty in the value of physical constants, 2) inaccuracy in geometric measurements and 3) instrument inaccuracies. The method employed herein to describe the uncertainty in the values reported is explained fully in Reference (14). However, before stating these uncertainties, an example of the process follows:

A theorem of statistics as stated in Reference (14) is:

"If R is a linear function of n dependent variables, each of which is normally distributed, then the relation between the interval for the variables, w_i, and the interval for the result, w_R, which gives the same odds for each of the variables and for the result is:

$$w_R = \left[\left(\frac{\partial R}{\partial v_1} w_1 \right)^2 + \left(\frac{\partial R}{\partial v_2} w_2 \right)^2 + \cdots + \left(\frac{\partial R}{\partial v_n} w_n \right)^2 \right]^{1/2}$$

where w_i = uncertainty interval based on certain odds.

Consider the Colburn j factor

$$j = N_{tu} \frac{Ac}{A} N_{PR}^{2/3}$$

by the theorem and letting $P = N_{PR}^{2/3}$

$$w_j = \left[\left(\frac{\partial j}{\partial N_{tu}} w_{N_{tu}} \right)^2 + \left(\frac{\partial j}{\partial A_c} w_{A_c} \right)^2 + \left(\frac{\partial j}{\partial A} w_A \right)^2 + \left(\frac{\partial j}{\partial P} w_P \right)^2 \right]^{1/2}$$

$$w_j = \left[\left(\frac{A_c}{A} \rho w_{N_{tu}} \right)^2 + \left(\frac{N_{tu} \rho}{A} w_{A_c} \right)^2 + \left(\frac{N_{tu} A_c \rho}{A^2} w_A \right)^2 + \left(\frac{2}{3} \frac{N_{tu} A_c}{A} \rho^{-1/3} w_P \right)^2 \right]^{1/2}$$

if both sides are divided by j then:

$$\frac{w_j}{j} = \left[\left(\frac{w_{N_{tu}}}{N_{tu}} \right)^2 + \left(\frac{w_{A_c}}{A_c} \right)^2 + \left(\frac{w_A}{A} \right)^2 + \left(\frac{2}{3} \frac{w_P}{P} \right)^2 \right]^{1/2} \qquad (1)$$

Before an equation such as this can be evaluated the uncertainty terms must be known.

The physical constants necessary are listed below. References (12) and (13) were sources for the values of these constants. The uncertainties in these values, as closely as can be determined, are also listed below.

c_s	$\pm$ 0.5%
c_p	$\pm$ 0.5%
μ	$\pm$ 1.0%
N_{PR}	$\pm$ 2.0%
k_s	$\pm$ 0.5%

The uncertainty in physical linear measurements could be considered negligible if core construction did not have minor inconsistencies. The uncertainty in the weight of a core is considered negligible. Conservative estimates of the uncertainty in linear measurements are:

A, A_{fr}, A_c, A_s,	$\pm$ 1.0%
L	$\pm$ 0.5%
W_s	< 0.1%

Instrumentation errors were such that only the manometers need be considered. With the exception of the orifice temperature, all temperatures measured were temperature differences and these were measured in inches as indicated in Appendix A. Since pressures varied and manometers to measure them changed, the maximum uncertainty encountered was used in the error analysis and is listed below.

P_o $\pm$ 1.25%

P_m $\pm$ 1.70%

P_{atm} negligible

Another uncertainty which requires special mention is that in N_{tu}. Since j does not vary linearly with N_R, the uncertainty at high and low N_R was considered. This uncertainty was determined by utilizing Figure 19 and the uncertainty in Maximum Slope as 2.0%.

$N_{tu} = 3.5, \quad \lambda = 0 \qquad \frac{dN_{tu}}{N_{tu}} = \pm 6.0\%$

$N_{tu} = 30, \quad \lambda = .04 \qquad \frac{dN_{tu}}{N_{tu}} = \pm 9.6\%$

Returning to Equation (1) and substituting as appropriate:

For high N_R: $\frac{w_j}{J} = \left[(.06)^2 + (.01)^2 + (.01)^2 + \left(\frac{.04}{3}\right)^2\right]^{1/2} = .063$ $\boxed{\frac{w_j}{J} = 6.3\%}$

For low N_R: $\frac{w_j}{J} = \left[(.096)^2 + (.01)^2 + (.01)^2 + \left(\frac{.04}{3}\right)^2\right]^{1/2} = .098$ $\boxed{\frac{w_j}{J} = 9.8\%}$

Following the above type of analysis, the following additional uncertainties were calculated.

$\dot{m}$ $\pm$ 1.0%

N_R $\pm$ 2.5%

f $\pm$ 4.3%

8. DISCUSSION OF RESULTS.

The 60 x 60 mesh screen matrix was used solely as a test matrix, a matrix whose heat transfer and friction characteristics were well documented. Figure 7 and Table I present the results. There is quite good agreement in the friction factor but a slight variation in j factor. This difference is attributed to the difference in the geometries of the test matrices. Exact reproduction of a screen matrix is difficult to achieve. The correlation was such that the experimental test setup was considered capable of delivering reliable data.

For further verification on the reliability of the test setup, Figures 8 to 10 and Tables II to IV present the test results for the Plate-Fin Reference Matrix, the 10° Skew Stainless Steel Matrix and the 20° Skew Stainless Steel Matrix used by Howard (6). Although this was not the original purpose for utilizing these matrices, the results do indicate conclusively that the "integral heater" is as good or better than the "sliding drawer" technique.

The original purpose for utilizing these matrices was to try and extend Howard's curves into the higher Reynold's number region (lower N_{tu} region). The points obtained in this region are plotted on the curves and the perinent data are recorded in the Tables. None of them follow the straight line of their predecessors. There are at least two reasons for this obvious departure from the norm. First, it is a well known fact that the "Maximum Slope" Method has an inherently large error in the low N_{tu} region of $1.5 \leq N_{tu} \leq 3.5$. This fact was originally published by Locke (1) for $\lambda = 0$. Howard (5) took into account longitudinal conduction and published an error curve that includes the effect of longitudinal conduction on an error in N_{tu}, see Figure 19. In the regions below $N_{tu} < 1.5$

the error is acceptable, yet, a discrepancy still exists. This points out the second reason for the discrepancy. The maximum slope at high flow rates (low N_{tu}) occurs at time t = 0+. Instrumentation prevents accurate measurement of the true maximum slope at this time due to inherent delay or lag time.

Extrapolation of the time-temperature curves back to time t = 0 was attempted in an effort to remove the effects of instrumentation. The method used was either incorrect or unreliable. Satisfactory results were unobtainable.

The merits of the plate-fin, 10° skew and 20° skew matrices as heat transfer surfaces was discussed thoroughly by Howard in reference (6).

Figures 11, 13 and 14 and Tables V, VI and VII present the results for a new geometry tested and a new idea in material. Figure 11 and Table V present the results for a 20° skew nickel matrix constructed from slotted plates. Appendix C explains fully the geometry of the slots and the calculations that determine the basic geometric parameters p, β, and r_H. The effects of longitudinal conduction was considered negligible as the matrix was constructed so that the air flow was normal to the long dimension of the slots. Plotting all the points uncorrected for conduction showed an erratic departure from the expected results for $N_R < 200$. It was then decided that perhaps the basic assumption was not warranted completely. Corrections for longitudinal conduction were made where significant and these points were plotted. These corrected values of j are overestimations, for, although A_s is corrected for the effects of the slots, the matrix length L is not the true conduction path length but at best a lesser approximation. Since λ is obviously not equal to zero,

the true value of j is probably between the uncorrected j ($\lambda = 0$) and the j corrected for longitudinal conduction using L as an approximation for conduction path length. This was considered in the interpretation of results.

Figure 12 compares the 20° skew stainless steel matrix with the perforated nickel matrix. There is a 70 to 100% increase in j, while f increases 10 to 25%.

It must be understood that these two matrices are geometrically similar only in overall dimensions. Actually, the heat transfer areas were calculated on different bases. The 20° skew stainless steel heat transfer area was based on the total surface area available for heat transfer while the heat transfer area of the 20° skew perforated was based on this same area less the area of the slots. Also, not included in the heat transfer area is the peripheral area of the slots normal to the flow. If the 20° skew perforated j factor were based on the total available area for heat transfer, the values plotted would be decreased approximately 40%. The perforated material still represents a substantial improvement in the performance. This improvement is attributed to the reduction of inefficient stagnant areas within the matrix and the alteration of the thermal and hydrodynamic boundary layers caused by the slots.

Figure 13 and Table VI present the results for a "parallel plate" matrix constructed from brass shim stock. As can be seen in Figure 13, the heat transfer performance falls far below that of theoretical laminar flow performance for parallel plates. Several things may account for this: the aspect ratio of the flow channels in this matrix was 77 vice ∞ for truly parallel plates, and also, the flow channels were not uniform in cross-section from one to another. The non-uniformity in cross-section

results in uneven mass flow through the matrix, hence inefficient use of the available heat transfer surfaces, and therefore a decrease in j.

The decrease in friction factor is possibly due to the sharp angle regions where the formed sections contact the flat plate. The wall shear stress in this type of region is small which would tend to reduce the value of f. These regions would also tend to produce stagnant regions previously mentioned, having a diminishing effect also on j.

Figure 14 and Table VII present the results for a "parallel plate" matrix constructed from perforated nickel plate. This matrix was constructed in the identical fashion as the brass matrix. Although it is not readily apparent in Figure 14, the heat transfer characteristics have been improved nearly 80%, while the friction factor has remained the same. Again it is necessary to make note of the fact that the heat transfer area of the two matrices were calculated on different bases. These bases are the same as discussed for the 20° skew matrices. Applicable also is the approximate reduction by 40% of the plotted values of the j factor if all of the area, in the perforated material, available for heat transfer, were considered in the calculations.

Figure 15 is a comparison of the two "parallel plate" matrices. The improvement realized by using perforated material is readily apparent, even considering the 40% reduction mentioned above. The additional performance gain in the transferral of heat is again attributed to the relieving of the stagnant areas and the alteration of the boundary layers caused by the slots.

The fact that the friction factor did not increase does not lend itself to previous conclusions (20° skew); that the presence of slots increases the friction factor. Some additional factor must be necessary.

Perhaps, the skewing coupled with the slots contribute more to friction than straight, slotted channels.

In the determination of the j factor for the perforated "parallel plate" matrix the conduction parameter, λ, was considered zero. Here again the plotted points departed from the expected straight line indicating that λ, in fact, was not zero. Corrections for longitudinal conduction were made using the matrix length, L, as an approximation for the conduction path length. These points were plotted also. Since the corrected points are overestimations and $\lambda \neq 0$, the true value of j lies between these limits.

The designer of a compact heat exchanger is generally restricted as to frontal area, volume, weight and pressure drop. There is presently coming into use, several means of comparing heat transfer surfaces with these restrictions in mind. Essentially, various parameters are compared graphically so that the relative merit of the various surfaces may be established.

The ratio j/f is plotted vs. Reynold's Number as a means of relating frontal flow area with pressure drop. For a given pressure drop a high j/f characteristic implies a small flow frontal area. j/f when plotted vs. N_R is known as the Flow Frontal Area "Goodness" factor.

The heat transfer power, h_{STD}, is plotted vs. the flow friction power, E_{STD}, and the resultant characteristic curve is a measure of relative core volumes. Generally, the surface with a high h_{STD} vs. E_{STD} characteristic will tend to have a small core volume. h_{STD} plotted in this fashion is known as the Volume "Goodness" factor.

Figure 16 compares the 20° skew matrices and the "parallel plate" matrices. Although the "Goodness" factors are not infallible, they are

indicative of relative performance. In this light, the perforated material should be excellent matrix material.

9. CONCLUSIONS.

Based upon the correlation of present data with that obtained by previous experimenters, the experimental test rig design presented herein is considered capable of producing reliable test data on the heat transfer and friction characteristics of a core module.

Basic heat transfer and flow friction characteristics for a new geometry and a new idea in material are presented in Figures 11 to 15. The geometric and physical properties are summarized in Figures 5 and 6. There appears to be a definite advantage to constructing matrices from perforated material. Performance is improved considerably and based on the "Goodness" factors (Figure 16) size and weight advantages are realized.

The 20° skew perforated nickel matrix was the top surface in performance. This matrix had the highest Flow Frontal Area "Goodness" factor, as well as the highest Volume to surface "Goodness" factor. This does not mean that this is the "optimum" surface for any given application but it does merit consideration.

In both geometries tested (20° skew and "parallel plate") the perforated material out-performed its counterpart. This would also indicate that further testing of this type of material (slotted) is warranted. It would seem that this material and some geometry should result in an outstanding heat exchanger surface.

10. RECOMMENDATIONS FOR FUTURE WORK.

1) Some means should be found to reliably determine N_{tu} in the high N_R range ($1.0 < N_{tu} < 3.5$). Most promising is the use of a periodic or cycling technique in which effectiveness is measured and used to find N_{tu} rather than the maximum slope. This ability is necessary if performance curves are to be extended to $N_R > 500$.

2) More work can be done with perforated material. Different geometries should be tested to see if consistantly high performances are realized as they have been in the past. Additionally, this type of surface is suspect of fouling. If these materials are as good as they seem to be, then examination of the effects of fouling on their performance is in order.

3) As more surfaces become available, they should be tested and their heat transfer and friction characteristics determined.

BIBLIOGRAPHY

1. G. L. LOCKE, "Heat Transfer and Flow Friction Characteristics of Porous Solids" TR - No. 10, Department of Mechanical Engineering, Stanford University, Stanford, California, June 1950.

2. T. E. W. SCHUMANN, "Heat Transfer: A Liquid Flowing Through A Porous Prism", Journal of the Franklin Institute, Vol. 208, p. 405 (1929).

3. F. A. CRESTWICK, "A Digital Computer Solution of the Equations for Transient Heating of a Porous Solid, Including the Effects of Longitudinal Conduction", Industrial Mathematics, Vol. 8, 1957, pp 61-69.

4. J. R. MONDT, "Effects of Longitudinal Thermal Conduction in the Solid on Apparent Convection Behavior, with Data For Plate Fin Surfaces", 1961 International Heat Transfer Conference, Boulder, Colorado, Paper No. 73, Proceedings, ASME.

5. C. P. HOWARD, "The Single Blow Problem Including the Effects of Longitudinal Conduction", ASME paper, No. 64-GTP-11.

6. C. P. HOWARD, "Heat Transfer and Flow Friction Characteristics of Skewed Passage and Glass - Ceramic Heat Transfer Surfaces". TR No. 59, Department of Mechanical Engineering, Stanford University, Stanford, California, October 1963.

7. "Chapter 4, Flow Measurement, Part 5 - Measurement of Quantity of Materials, American Society of Mechanical Engineers, 1959.

8. W. M. KAYS and A. L. LONDON, "Compact Heat Exchangers", McGraw-Hill Book Company, New York, New York, 1959.

9. J. E. COPPAGE, "Heat Transfer and Flow Friction Characteristics of Porous Media", TR No. 16, Department of Mechanical Engineering, Stanford University, Stanford, California, December, 1952.

10. SOLAR ENGINEERING REPORT ER 1221, "Regenerator Core Module Thermal Tests - T-600 Engine", 18 April 1962. Rev. A: 25 October, 1962, AD 290234.

11. F. E. MORELAND, "Solution of the Single Blow Problem, with Longitudinal Conductivity by Numerical Inversion of LaPlace Transforms," Master's Thesis, U. S. Naval Postgraduate School, Monterey, California, 1964.

12. HILSENRATH, J., et al., "Tables of Thermal Properties of Gases," U. S. Department of Commerce, National Bureau of Standards, Circular 564, November, 1955.

13. GOLDSMITH, A., et al., "Handbook of Thermophysical Properties of Solid Materials," Revised Edition, Vol. II, Alloys, Macmillan Co., 1961, pp 159-162, pp 333-336, and pp 443-450.

14. S. J. KLINE and F. A. McCLINTOCK, "Describing Uncertainties in Single Sample Experiments," Mechanical Engineering, January 1953.

15. A. L. LONDON, "New Developments in Compact Heat Exchanges, Design, Theory, Surfaces, and Applications" Mechanical Engineering, May 1964.

16. C. C. FURNAS, "Heat Transfer from a Gas Stream to a Bed of Broken Solids," U. S. Bureau of Mines Bulletin No. 361 (1932).

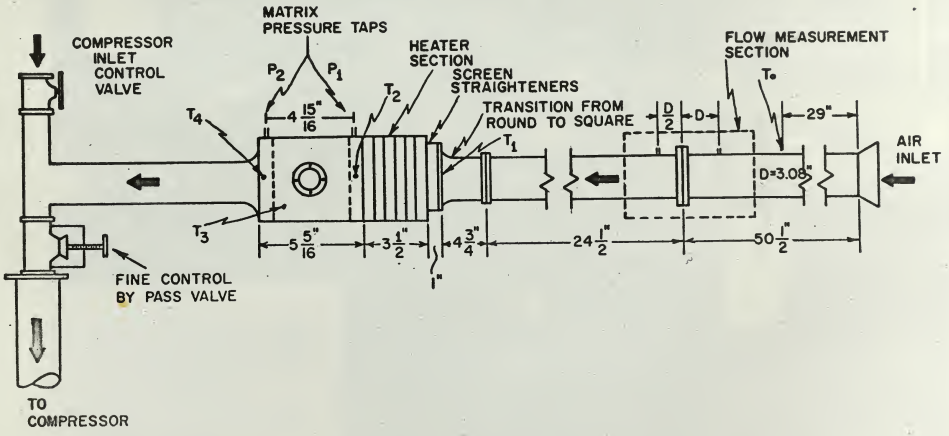

FIGURE 1. SCHEMATIC DIAGRAM OF TEST APPARATUS

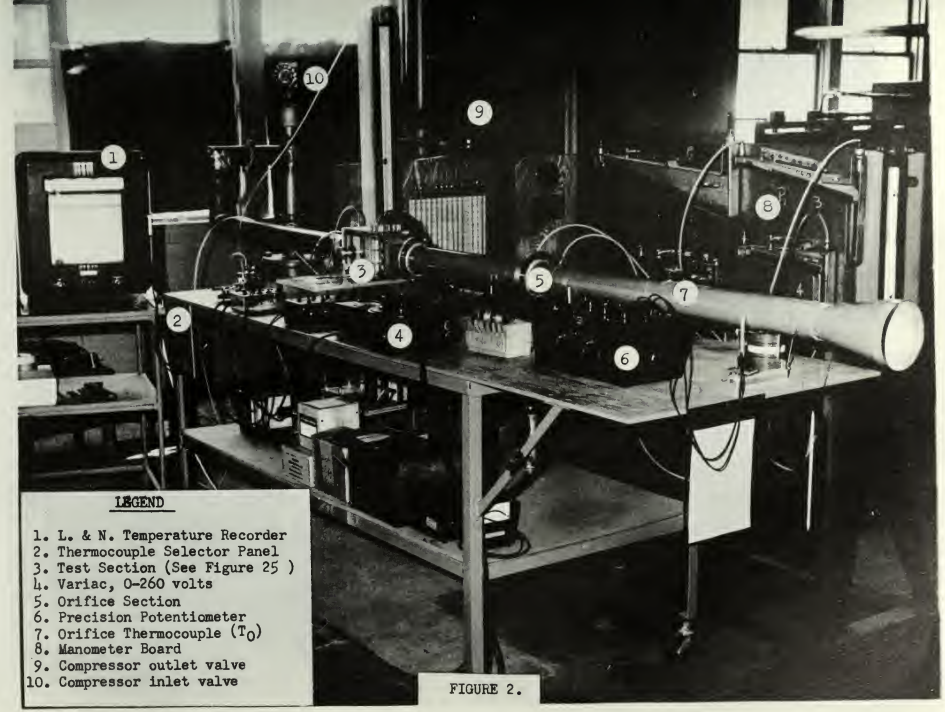

LEGEND

1. L. & N. Temperature Recorder
2. Thermocouple Selector Panel
3. Test Section (See Figure 25)
4. Variac, 0-260 volts
5. Orifice Section
6. Precision Potentiometer
7. Orifice Thermocouple (T_O)
8. Manometer Board
9. Compressor outlet valve
10. Compressor inlet valve

FIGURE 2.

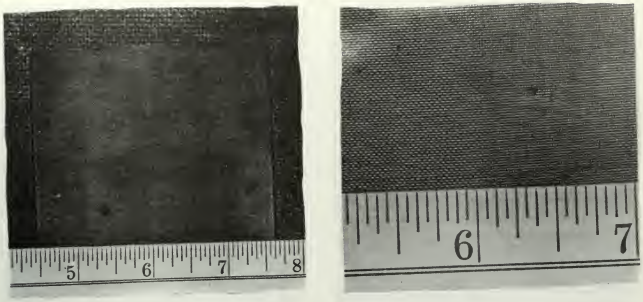

Matrix Material	18-8 St. Steel
Specific Heat (c_s) BTU/lb °F	0.12
Thermal Conductivity (k_s) BTU/hr °F ft	10.0
Material Thickness, inches	0.017
Total Heat Transfer Area (A) ft^2	4.0159
Frontal Area (A_{fr}) ft^2	0.07055
Total Conduction Area (A_s) ft^2	0.02215
Flow Cross Section Area (A_c) ft^2	0.0484
Matrix Volume (V_m) ft^3	0.00199
Matrix Density (ρ_m) lb/ft^3	155.
Hydraulic Diameter (D_H) ft	0.00136
Compactness (β) ft^2/ft^3	2009.
Porosity (p)	0.686

FIGURE 3 Physical and Geometric Properties of 60x60 Mesh Screen Matrix

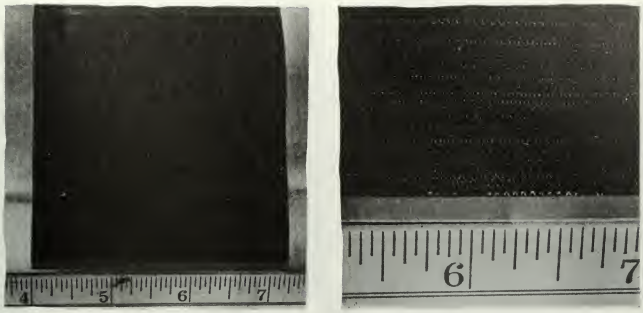

Matrix Material	Type 302 S. Steel
Specific Heat (c_s) BTU/lb °F	0.11
Thermal Conductivity (k_s) BTU/hr °F ft	7.0
Material Thickness, inches	0.001
Total Heat Transfer Area (A) ft^2	30.12
Frontal Area (A_{fr}) ft^2	0.07023
Total Conduction Area (A_s) ft^2	0.00752
Flow Cross Section Area (A_c) ft^2	0.06271
Matrix Volume (V_m) ft^3	0.01170
Matrix Density (ρ_m) lb/ft^3	52.9
Hydraulic Diameter (D_H) ft	.001388
Compactness (β) ft^2/ft^3	2573.
Porosity (p)	0.893

FIGURE 4 Physical and Geometric Properties of Plate-Fin Reference Matrix

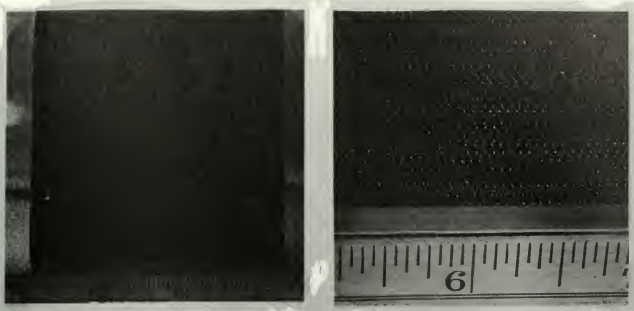

Matrix Material	10° SKEW Type 302 S.Steel	20° SKEW Type 302 S.Steel	20° SKEW perf. Nickel
Specific Heat (c_s) BTU/lb °F	0.11-	0.11	0.1065
Thermal Cond. (k_s) BTU/hr °F ft	7.0	7.0	38.7
Material Thickness, inches	0.001	0.001	0.0022
Total Heat Transfer Area (A) ft^2	18.38	18.04	15.41
Frontal Area (A_{fr}) ft^2	0.07024	0.0702	0.0734
Total Conduction Area (A_s) ft^2	0.00464	0.00452	0.00349
Flow Cross Section Area (A_c) ft^2	0.0656	0.0657	0.06412
Matrix Volume (V_m) ft^3	0.0117	0.01157	0.01211
Matrix Density (ρ_m) lb/ft^3	32.4	32.22	50.1
Hydraulic Diameter (D_H) ft	.002381	.002416	.002528
Compactness (β) ft^2/ft^3	1570.	1549.	1272.
Porosity (p)	0.934	0.936	0.873

FIGURE 5 Physical and Geometric Properties of Skew Matrices

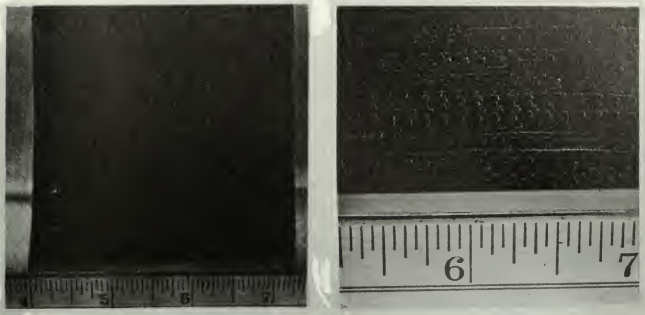

Matrix Material	70-30 Brass	Perf. Nickel
Specific Heat (c_s) BTU/lb °F	0.092	0.1065
Thermal Conductivity (k_s) BTU/hr °F ft	66.	38.7
Material Thickness, inches	0.001	0.0022
Total Heat Transfer Area (A) ft^2	22.057	18.586
Frontal Area (A_{fr}) ft^2	0.06986	0.0695
Total Conduction Area (A_s) ft^2	0.00551	0.00416
Flow Cross Section Area (A_c) ft^2	0.06434	0.0584
Matrix Volume (V_m) ft^3	0.01164	0.01158
Matrix Density (ρ_m) lb/ft^3	41.5	63.6
Hydraulic Diameter (D_H) ft	.001944	.001928
Compactness (β) ft^2/ft^3	1895.	1605.
Porosity (p)	.921	.840

FIGURE 6 Physical and Geometric Properties of "Parallel Plate" Matrices

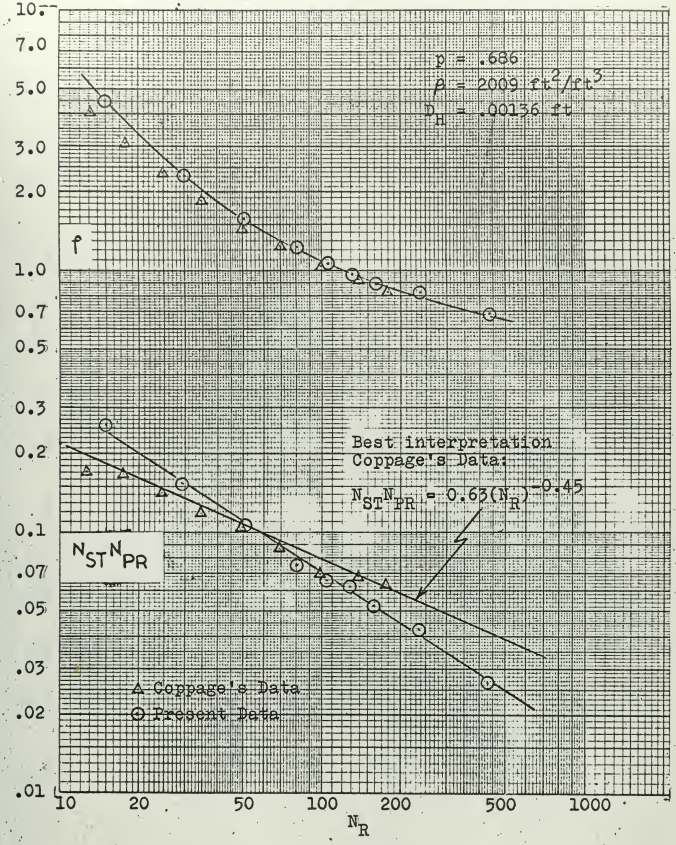

Figure 7 60x60 Mesh Stainless Steel Screens

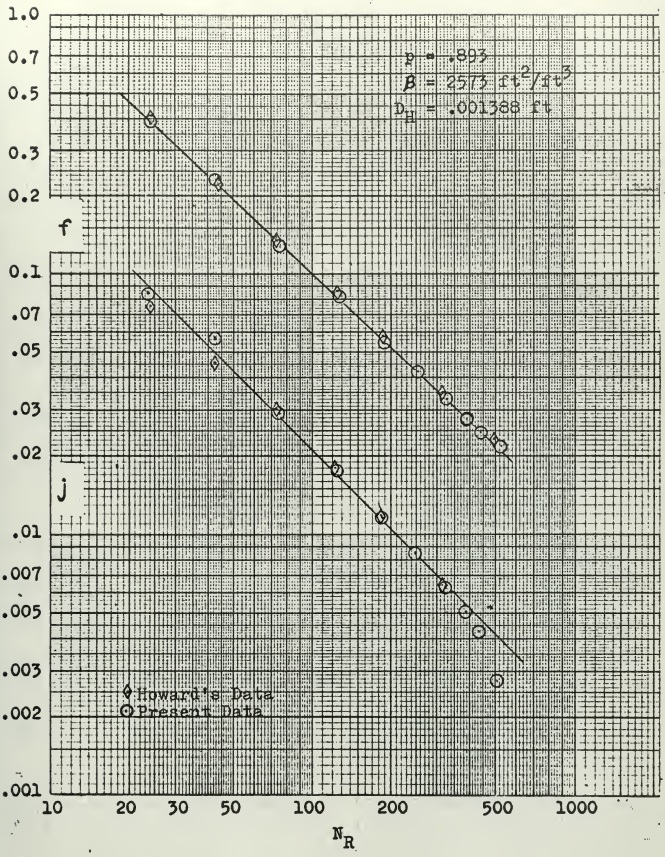

Figure 8 Plate Fin Reference Matrix

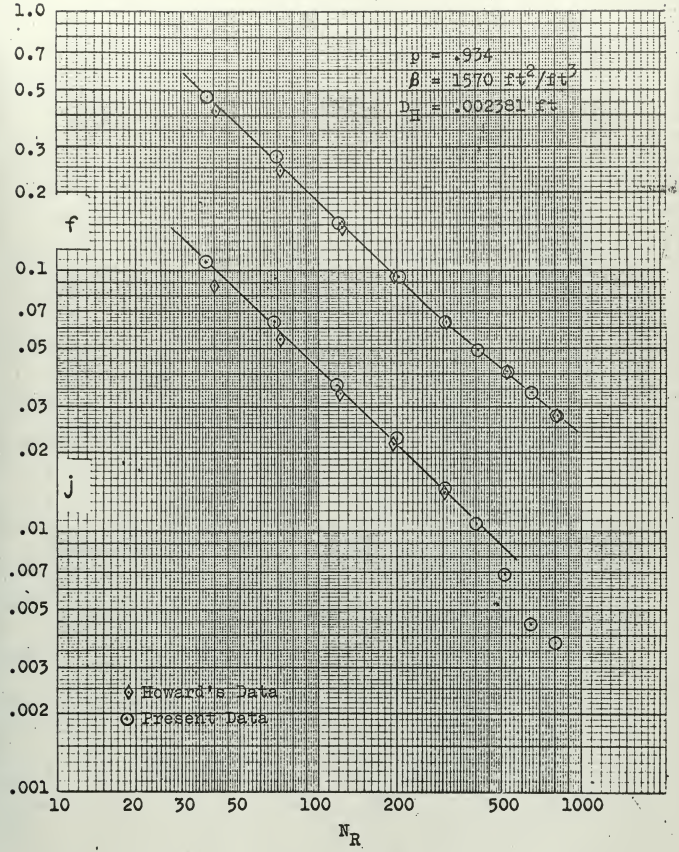

Figure 9 10° Skew Stainless Steel Matrix

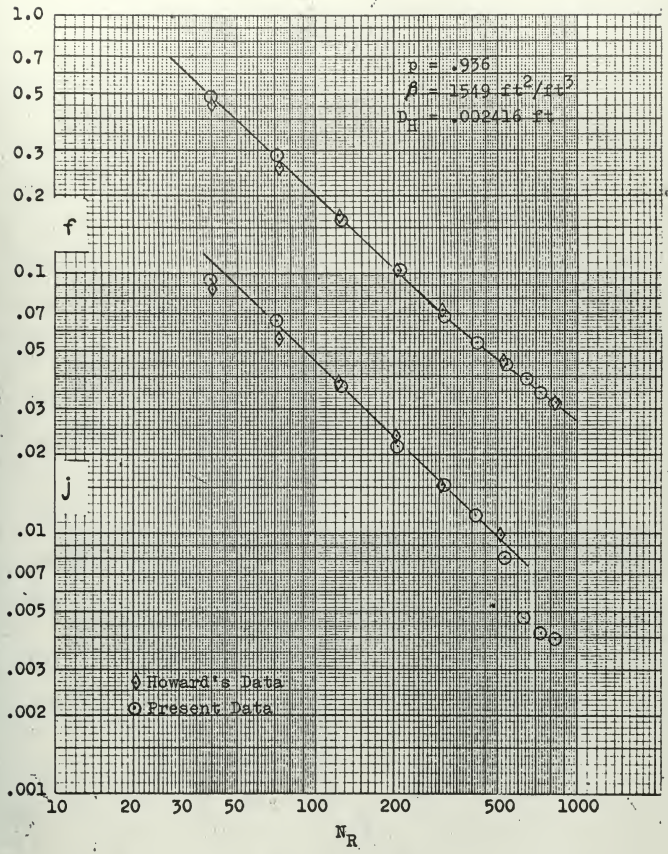

Figure 10 20° Skew Stainless Steel Matrix

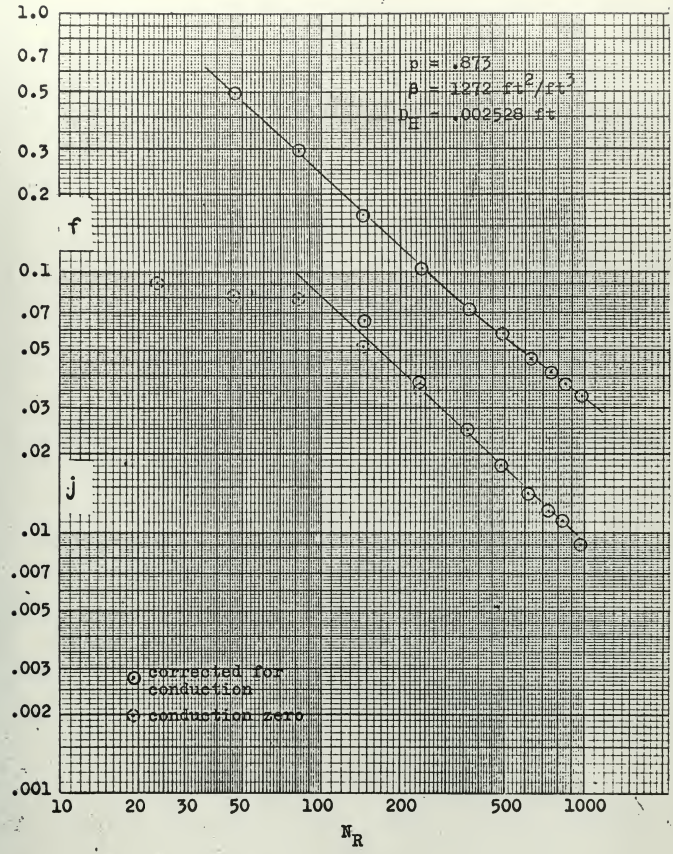

Figure 11 20° Skew Nickel (Perforated) Matrix

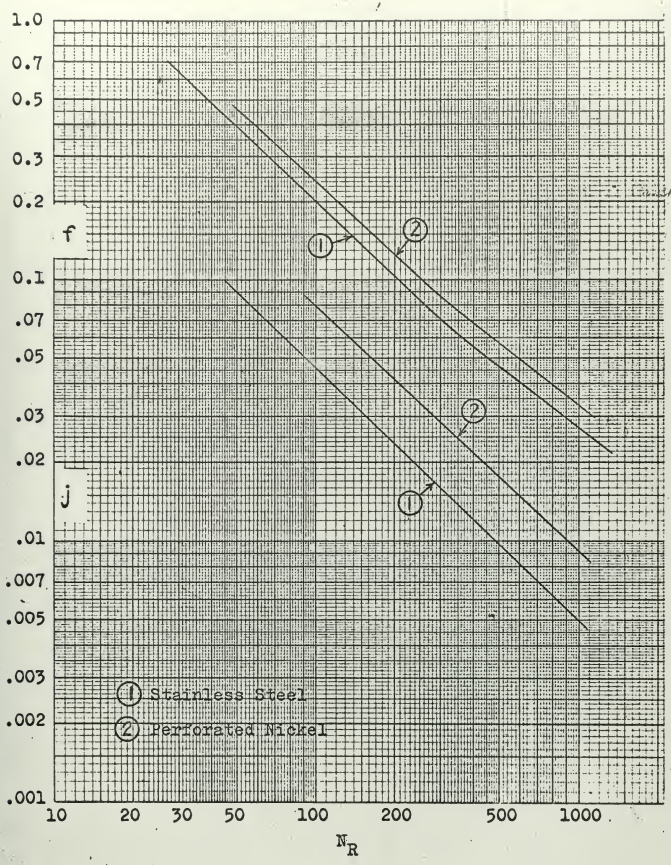

Figure 12 Comparison of perforated and non-perforated 20° Skew Matrices

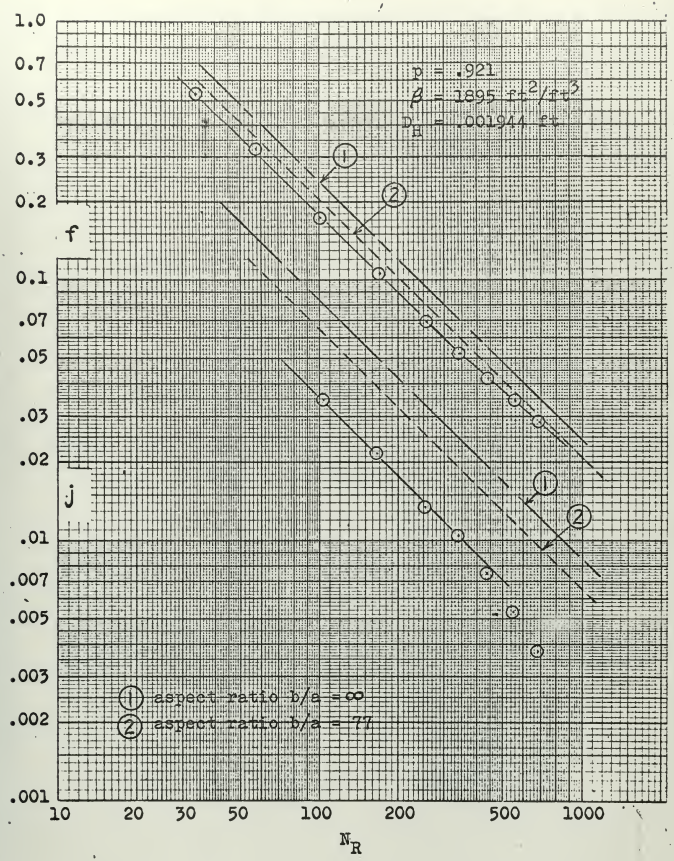

Figure 13 "Parallel Plate" Brass Matrix

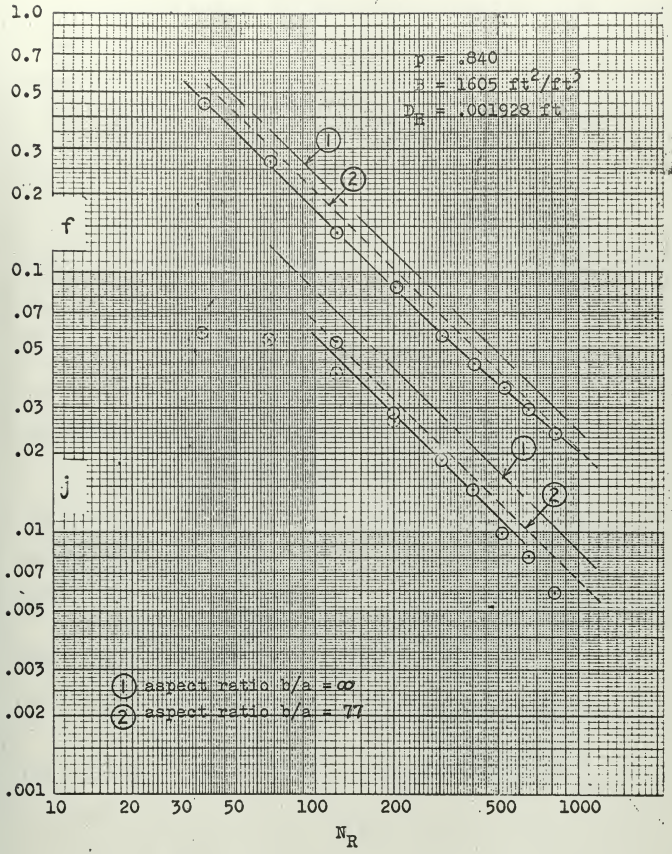

Figure 14 "Parallel Plate" Nickel (perforated) Matrix

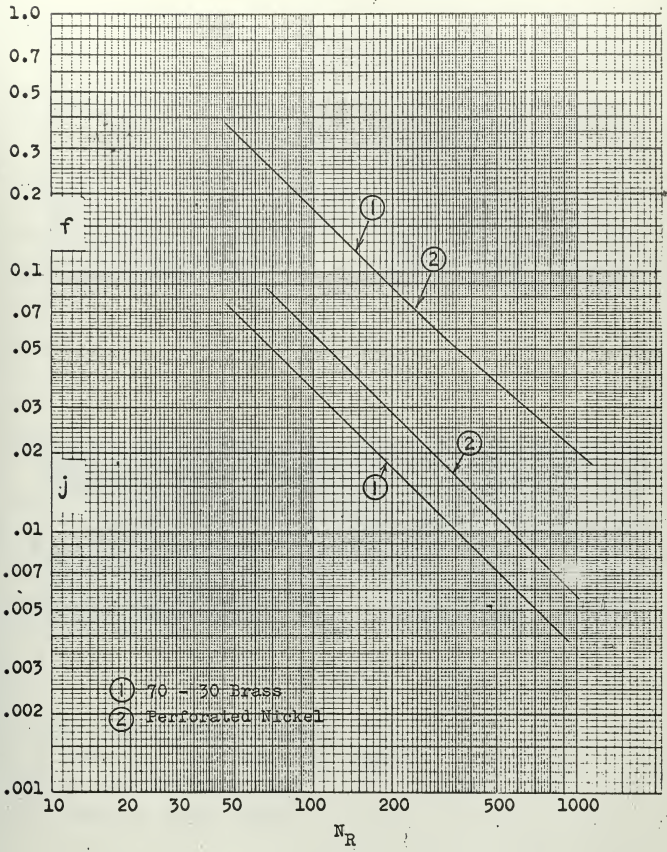

Figure 15 Comparison of Perforated and non-perforated "Parallel Plate" Matrices

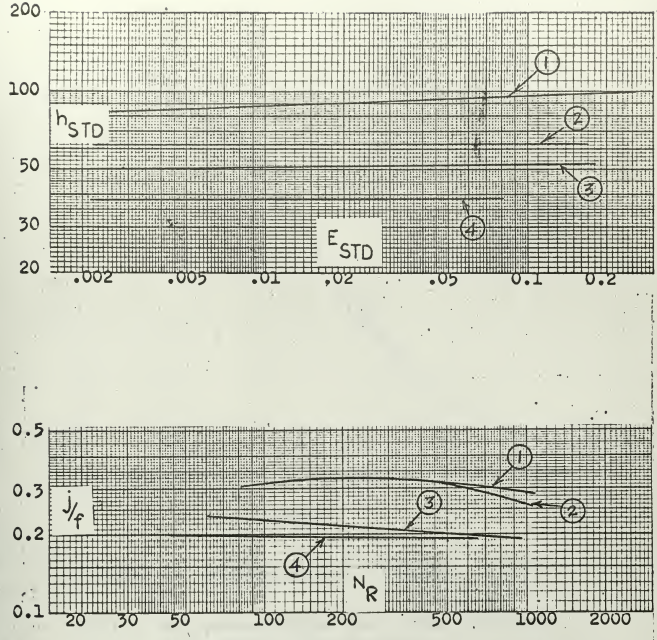

(1) 20° Skew Perforated Nickel
(2) "Parallel Plate" Perforated Nickel
(3) 20° Skew Stainless Steel
(4) "Parallel Plate" Brass

Figure 16 Design "Goodness" Factors

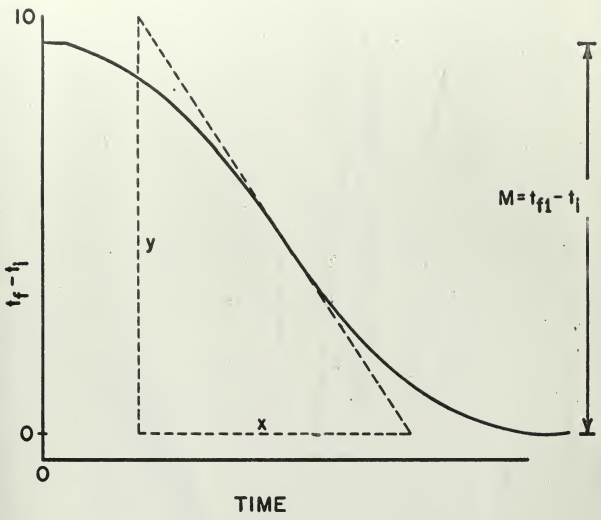

FIGURE 17. GENERALIZED COOLING CURVE

NOTE: All measurements are made in inches to facilitate computations.

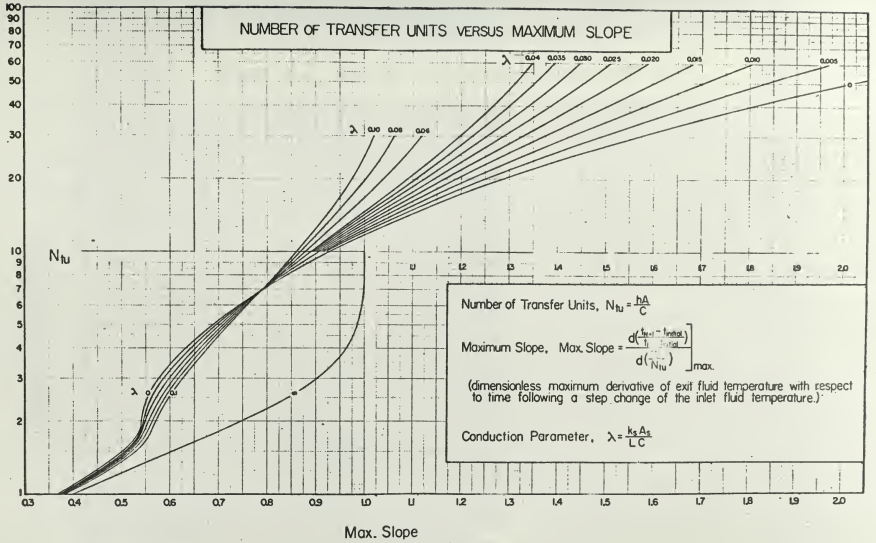

Figure 18 Number of Transfer Units (N_{tu}) vs. Maximum Slope

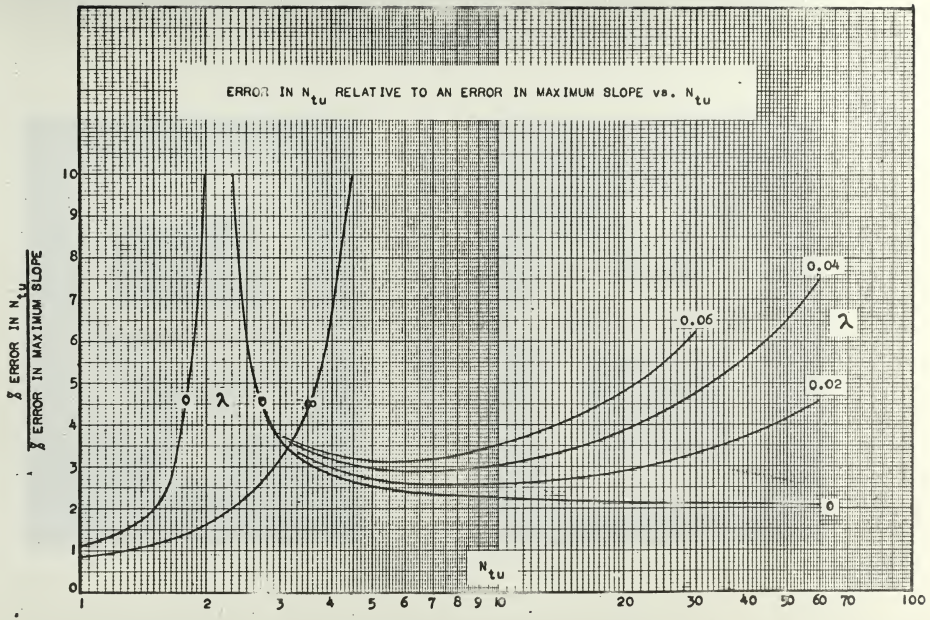

Figure 19 Error in N_{tu} relative to an error in Maximum Slope vs. N_{tu}

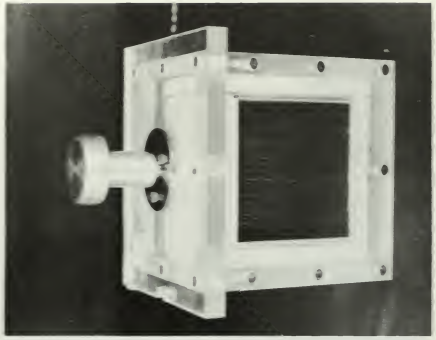

FIGURE 20. Matrix Holder (Upstream View)

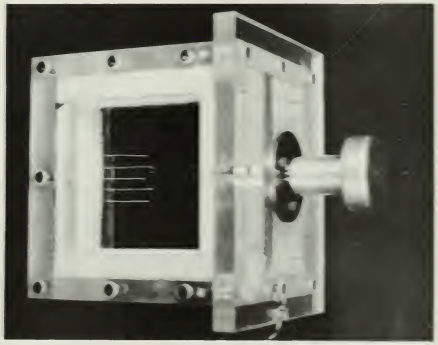

FIGURE 21. Matrix Holder (Downstream View)

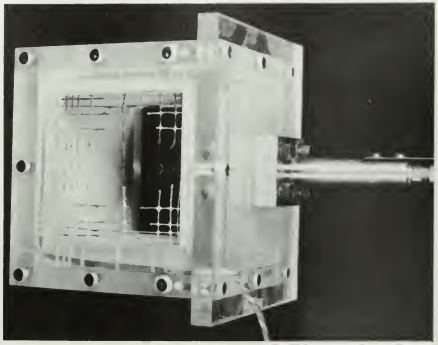

FIGURE 22. Matrix Holder modified with probe for velocity profile measurement and temperature distribution measurement (Downstream View)

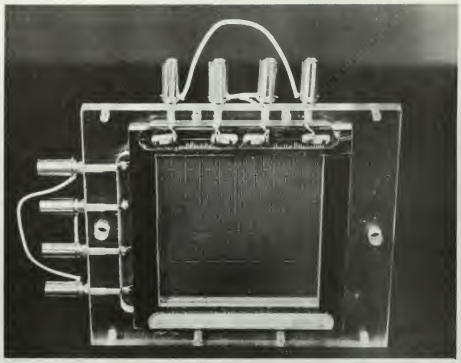

FIGURE 23. Nichrome Wire Heater (Upstream View)

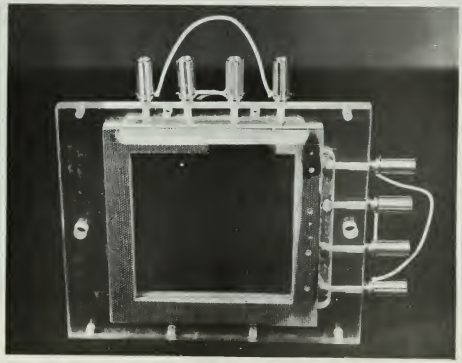

FIGURE 24. Nichrome Wire Heater (Downstream View)

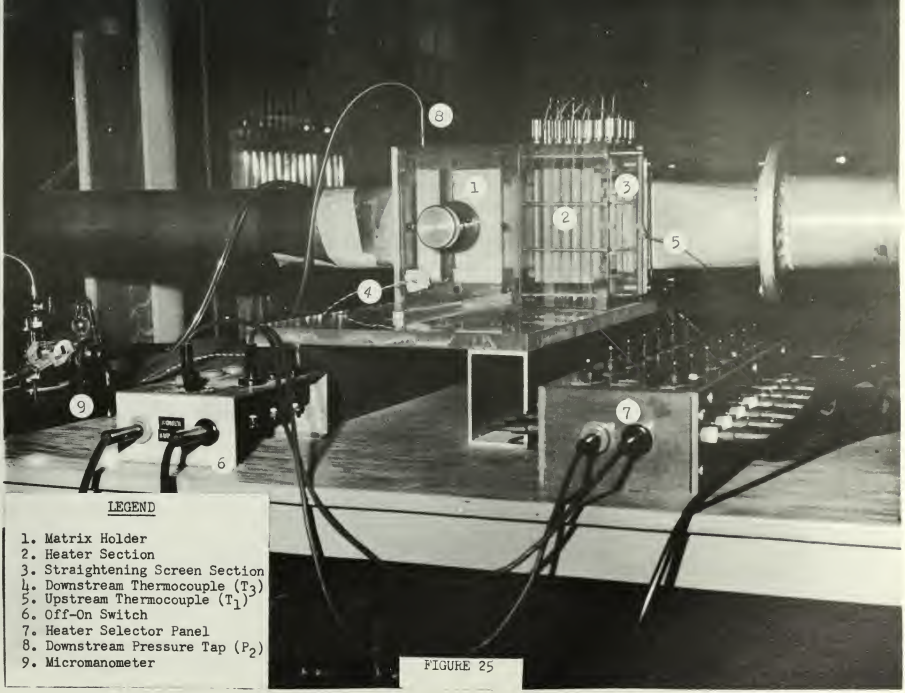

LEGEND

1. Matrix Holder
2. Heater Section
3. Straightening Screen Section
4. Downstream Thermocouple (T_3)
5. Upstream Thermocouple (T_1)
6. Off-On Switch
7. Heater Selector Panel
8. Downstream Pressure Tap (P_2)
9. Micromanometer

FIGURE 25

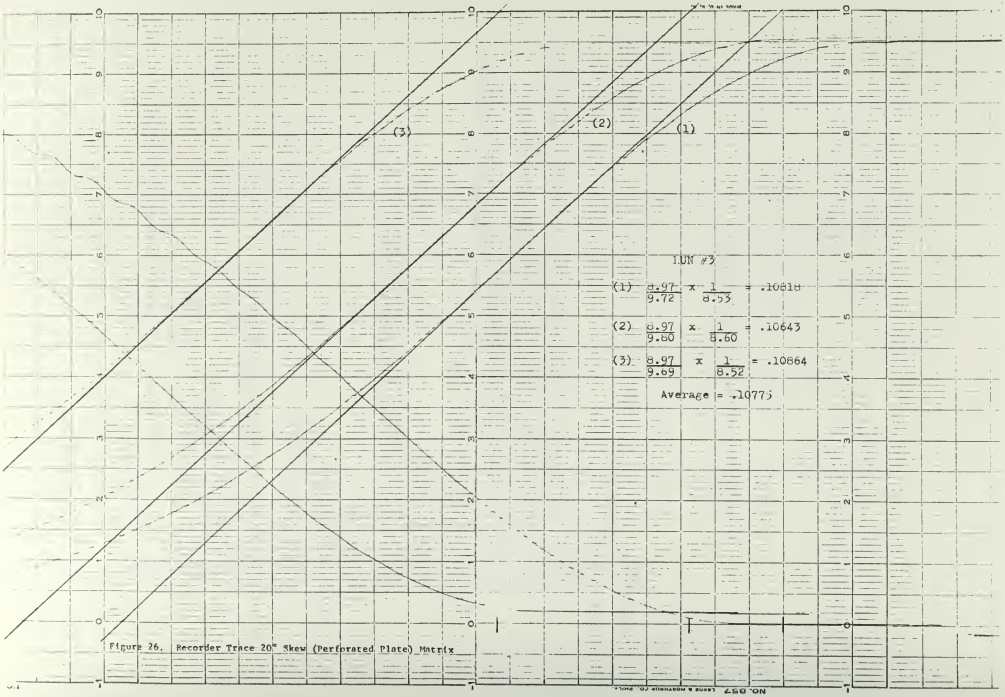

Figure 26. Recorder Trace 20° Skew (Perforated Plate) Matrix

```
      PROGRAM MAXSLO
      L=2
      K=1
   30 READ 300,XML,AS,RH,POR,AFL,AHT,WM
  300 FORMAT(7F10.5)
   40 READ 400,EK,CK,SK,CM,N
  400 FORMAT(4F10.5,12)
      M=1
   10 READ 100,DO,DELPO,GAM,ATMP,COR,UH,UFR
  100 FORMAT(7F10.5)
      READ 101,CS,DELH ,HS,SLO,TEMPO
  101 FORMAT(5F10.5)
      EMDOT=359.0*DO*DO*SQRTF(DELPO*GAM*ATMP/29.92)*COR
      CP=0.24
      RNUMP=5.09*EMDOT/UFR
      RNUMH=(4.0*XML*EMDOT)/(AHT*UH)
      RNUMFR=RNUMH*UH/UFR
      CAPFL=EMDOT*CP/3600.0
      CAPS=WM*CM
      SLOMAX=(CAPS*SLO)/(CAPFL*CS)
      CONDPAR=(SK*AS)/(XML*EMDOT*CP)
      B=CK+EK
      C=1.0+POR**2
      G=EMDOT/(AFL*3600.0)
      DELP=DELH*.03613
      PS=HS*.03613
      PA=ATMP*.4912
      P1=PA-PS
      P2=P1-DELP
      PM=(P1+P2)/2.
      RHOM=(PM*144.0)/(53.3*(TEMPO+460.0))
      FF1=((64.4*RHOM*DELP*144.0)/(G*G))
      FF2=C*DELP/PM
      FF3=FF1-FF2-B
      FFR=FF3*RH/XML
      WRITE OUTPUT TAPE 4,4,M
    4 FORMAT(9H RUN NO. I2///)
      WRITE OUTPUT TAPE 4,1,EMDOT,RNUMP,RNUMH,CAPFL,CAPS
    1 FORMAT(7H EMDOT=F10.5,3X,7H RNUMP=E20.8,3X,7H RNUMH=F10.5,3X,
     17H CAPFL=F10.5,3X,6H CAPS=F10.5///)
      WRITE OUTPUT TAPE 4,2,CONDPAR,SLOMAX
    2 FORMAT(9H CONDPAR=F10.5,3X,8H SLOMAX=F10.5///)
      WRITE OUTPUT TAPE 4,3,G,RNUMFR,FFR
    3 FORMAT(3H G=F10.5,3X,8H RNUMFR=F10.5,3X,5H FFR=F10.5/)
      M=M+1
      IF(N-M)50,10,10
   50 K=K+1
      IF(L-K)20,30,30
   20 STOP
      END
      END
```

Figure 27 Program MaxSlo Readout

TABLE I SUMMARY OF HEAT TRANSFER AND FRICTIONAL RESULTS:
60x60 MESH STAINLESS STEEL SCREEN MATRIX

HEAT TRANSFER RESULTS:

RUN #	REYNOLD'S NUMBER	$N_{ST}N_{PR}$	CONDUCTION PARAMETER	MAXIMUM SLOPE	N_{tu}
1	431.57	.0267	0.0	.58333	3.12
2	234.81	.0425	0.0	.68566	4.96
3	159.26	.0521	0.0	.74639	6.09
4	129.69	.0620	0.0	.80395	7.25
5	106.78	.0659	0.0	.82926	7.77
6	79.88	.0755	0.0	.87817	8.83
7	50.69	.1040	0.0	1.05579	11.90
8	29.60	.1535	0.0	1.22105	17.94
9	15.43	.2584	0.0	1.57029	30.19
10	8.49	.4760	0.0	2.11897	55.65

ISOTHERMAL FRICTION RESULTS:

RUN #	REYNOLD'S NUMBER	FRICTION FACTOR
1	437.93	.68548
2	238.27	.82196
3	161.60	.89263
4	131.60	.97400
5	108.36	1.06410
6	81.07	1.23243
7	51.44	1.57979
8	30.04	2.31547
9	15.66	4.47090
10	8.62	9.50629

TABLE II SUMMARY OF HEAT TRANSFER AND FRICTIONAL RESULTS:

PLATE-FIN REFERENCE MATRIX

HEAT TRANSFER RESULTS:

RUN #	REYNOLD'S NUMBER N_R	$N_{ST}N_{PR}^{2/3}$ j	CONDUCTION PARAMETER λ	MAXIMUM SLOPE	N_{tu}	N_{tu} (λ=0)
1	505.17	.00277	.00128	.52583	1.68	1.68
2	433.26	.00429	.00150	.55712	2.60	2.60
3	387.19	.00505	.00167	.58044	3.06	3.06
4	322.08	.00634	.00201	.62383	3.84	3.84
5	248.92	.00842	.00260	.69377	5.10	5.10
6	187.25	.01162	.00346	.79434	7.04	7.04
7	125.74	.01761	.00515	.94678	10.67	10.44
8	75.04	.02889	.00862	1.16341	17.51	16.21
9	42.68	.05699	.01516	1.43365	34.54	25.07
10	23.81	.08403	.02717	1.43851	50.93	25.22

ISOTHERMAL FRICTION RESULTS:

RUN #	REYNOLD'S NUMBER N_R	FRICTION FACTOR f
1	512.59	.02197
2	439.62	.02485
3	392.86	.02795
4	326.79	.03304
5	252.57	.04210
6	189.99	.05433
7	127.58	.08205
8	76.14	.12974
9	43.30	.23164
10	24.17	.39637

TABLE III SUMMARY OF HEAT TRANSFER AND FRICTIONAL RESULTS: 10° SKEW STAINLESS STEEL MATRIX

HEAT TRANSFER RESULTS:

RUN #	REYNOLD'S NUMBER N_R	$N_{ST}N_{PR}^{2/3}$ j	CONDUCTION PARAMETER λ	MAXIMUM SLOPE	N_{tu}	N_{tu} (λ=0)
1	805.27	.00375	.00081	.46533	1.32	1.32
2	643.32	.00440	.00101	.51088	1.55	1.55
3	517.86	.00695	.00126	.55129	2.45	2.45
4	402.58	.01073	.00162	.62114	3.78	3.78
5	305.00	.01488	.00214	.70167	5.24	5.24
6	200.72	.02271	.00324	.83894	8.00	7.98
7	119.58	.03642	.00544	1.02840	12.83	12.46
8	68.74	.06376	.00953	1.27448	22.46	19.62
9	37.61	.10788	.01728	1.44693	38.00	25.53

ISOTHERMAL FRICTION FACTOR:

RUN #	REYNOLD'S NUMBER N_R	FRICTION FACTOR f
1	817.04	.02791
2	652.71	.03405
3	525.43	.04092
4	408.46	.04951
5	309.46	.06345
6	203.79	.09412
7	121.41	.15138
8	70.00	.27472
9	38.16	.47276

TABLE IV SUMMARY OF HEAT TRANSFER AND FRICTIONAL RESULTS:

20° SKEW STAINLESS STEEL MATRIX

HEAT TRANSFER RESULTS:

RUN #	REYNOLD'S NUMBER N_R	$N_{ST}N_{PR}^{2/3}$ j	CONDUCTION PARAMETER λ	MAXIMUM SLOPE	N_{tu}	N_{tu} (λ=0)
1	835.38	.00394	.00078	.47359	1.36	1.36
2	728.65	.00414	.00090	.48768	1.43	1.43
3	636.57	.00475	.00103	.52394	1.64	1.64
4	535.10	.00805	.00122	.56474	2.78	2.78
5	412.85	.01182	.00158	.63657	4.09	4.09
6	312.06	.01524	.00209	.70256	5.26	5.26
7	208.65	.02167	.00313	.81581	7.48	7.48
8	126.47	.03676	.00517	1.02339	12.69	12.33
9	71.21	.06593	.00917	1.28940	22.76	20.09
10	39.79	.09441	.01646	1.39790	32.59	23.79

ISOTHERMAL FRICTION FACTOR:

RUN #	REYNOLD'S NUMBER N_R	FRICTION FACTOR f
1	848.11	.03197
2	739.39	.03471
3	645.95	.03908
4	542.97	.04465
5	418.94	.05431
6	316.65	.06856
7	211.73	.10255
8	128.33	.16015
9	72.26	.28784
10	40.40	.48428

TABLE V SUMMARY OF HEAT TRANSFER AND FRICTIONAL RESULTS:

20° SKEW NICKEL MATRIX (PERFORATED PLATES)

HEAT TRANSFER RESULTS:

RUN #	REYNOLD'S NUMBER N_R	$N_{ST}N_{PR}^{2/3}$ j	CONDUCTION PARAMETER λ	MAXIMUM SLOPE	N_{tu}	N_{tu} (λ=0)
1	966.07	.00900	.00337	.56394	2.72	2.72
2	835.43	.01146	.00390	.60157	3.42	3.46
3	738.42	.01219	.00441	.61776	3.70	3.68
4	619.79	.01418	.00526	.64762	4.24	4.28
5	484.37	.01802	.00674	.71212	5.41	5.44
6	362.97	.02497	.00898	.81813	7.58	7.54
7	239.79	.03517	.01359	.95653	11.29	10.62
8	145.03	.05199	.02243	1.14669	19.65	15.70
9	82.26	.07879	.03951	1.39808	-	23.79
10	46.22	.08147	.07039	1.42079	-	24.60
11	23.50	.09134	.13843	1.50225	-	27.58

ISOTHERMAL FRICTION FACTOR:

RUN #	REYNOLD'S NUMBER N_R	FRICTION FACTOR f
1	980.29	.03316
2	847.72	.03709
3	749.28	.04116
4	628.91	.04686
5	491.63	.05802
6	368.31	.07208
7	243.32	.10258
8	147.16	.16737
9	83.46	.29667
10	46.89	.49889
11	23.85	1.09090

TABLE VI SUMMARY OF HEAT TRANSFER AND FRICTIONAL RESULTS:

"PARALLEL PLATE" BRASS MATRIX

HEAT TRANSFER RESULTS:

RUN #	REYNOLD'S NUMBER N_R	$N_{ST}N_{PR}^{2/3}$ j	CONDUCTION PARAMETER λ	MAXIMUM SLOPE	N_{tu}	N_{tu} (λ=0)
1	683.97	.00376	.00896	.49410	1.44	1.46
2	551.23	.00527	.01112	.54861	2.27	2.40
3	437.55	.00748	.01401	.59598	3.22	3.36
4	340.15	.01038	.01802	.66717	4.47	4.63
5	255.77	.01335	.02390	.73472	5.75	5.63
6	168.67	.02148	.03634	.87166	9.25	8.71
7	102.18	.03483	.05999	.97562	15.00	11.15
8	57.06	-	.10761	1.07854	-	-
9	33.37	-	.18369	.98829	-	-

ISOTHERMAL FRICTION FACTOR:

RUN #	REYNOLD'S NUMBER N_R	FRICTION FACTOR f
1	694.19	.02846
2	559.46	.03454
3	444.09	.04292
4	345.24	.05240
5	259.52	.06907
6	171.19	.10680
7	103.71	.17239
8	57.90	.32370
9	33.86	.53085

TABLE VII SUMMARY OF HEAT TRANSFER AND FRICTIONAL RESULTS:

"PARALLEL PLATE" NICKEL MATRIX (PERFORATED PLATES)

HEAT TRANSFER RESULTS:

RUN #	REYNOLD'S NUMBER N_R	$N_{ST}N_{PR}^{2/3}$ j	CONDUCTION PARAMETER λ	MAXIMUM SLOPE	N_{tu}	N_{tu} (λ=0)
1	819.49	.00590	.00393	.54781	2.32	2.36
2	647.21	.00810	.00497	.58864	3.18	3.24
3	518.89	.00988	.00620	.62923	3.89	3.95
4	400.50	.01458	.00804	.73180	5.77	5.83
5	304.49	.01891	.01058	.81941	7.61	7.56
6	200.68	.02659	.01602	.95459	11.31	10.63
7	121.15	.04039	.02658	1.16142	21.61	16.15
8	67.53	.05502	.04768	1.34786	-	22.00
9	37.92	.04945	.08478	1.27951	-	19.70

ISOTHERMAL FRICTION FACTOR:

RUN #	REYNOLD'S NUMBER N_R	FRICTION FACTOR f
1	831.56	.02395
2	656.72	.02955
3	526.51	.03577
4	406.49	.04439
5	309.04	.05682
6	203.63	.08725
7	122.96	.14242
8	68.54	.26776
9	38.48	.45874

N_{tu} \ λ	Maximum Slope														
	0	.005	.010	.015	.020	.025	.030	.035	.040	.060	.080	.100	.500	1.0	10	∞
1.0	.368	-	-	-	.374	-	-	-	.377	.380	.382	.384	-	-	-	.400
1.1	.403	-	-	-	.408	-	-	-	.413	.417	.420	.425	-	-	-	.445
1.2	.434	-	-	-	.440	-	-	-	.445	.447	.452	.459	-	-	-	.488
1.3	.461	-	-	-	.467	-	-	-	.472	.475	.480	.487	.497	-	-	.529
1.4	.483	-	-	-	.489	-	-	-	.494	.498	.503	.511	.522	-	-	.568
1.5	.502	-	-	-	.507	-	-	-	.512	.517	.521	.530	.542	-	-	.603
1.6	.517	-	-	-	.522	-	-	-	.527	.530	.536	.544	.560	-	-	.637
1.8	.536	-	-	-	.539	-	-	-	.542	.547	.553	.561	.589	-	-	.697
2.0	.541	-	-	-	.545	-	-	-	.548	.556	.563	.571	.615	.646	.723	.748
2.2	.544	-	-	-	.549	-	-	-	.557	.566	.574	.582	.640	.677	.764	.791
2.4	.549	-	-	-	.557	-	-	-	.567	.577	.585	.592	.662	.703	.798	.827
2.6	.557	-	-	-	.566	-	-	-	.577	.587	.595	.603	.682	.726	.826	.857
2.8	.567	-	-	-	.577	-	-	-	.587	.598	.606	.615	.699	.745	.850	.882
3.0	.577	-	-	-	.587	-	-	-	.598	.608	.617	.626	.714	.761	.869	.903
3.2	.587	-	-	-	.598	-	-	-	.609	.619	.628	.637	.727	.775	.886	.920
3.4	.598	-	-	-	.610	-	-	-	.620	.630	.640	.647	.738	.787	.899	.934
3.6	.609	-	-	-	.621	-	-	-	.631	.641	.650	.658	.749	.798	.911	.946
3.8	.621	-	-	-	.632	-	-	-	.642	.652	.660	.668	.758	.807	.920	.956
4.0	.632	-	-	-	.643	-	-	-	.653	.662	.670	.678	.767	.815	.928	.964
4.5	.660	-	-	-	.670	-	-	-	.678	.687	.694	.701	.784	.831	.941	.978
5.0	.688	-	-	-	.697	-	-	-	.704	.711	.717	.722	.800	.843	.951	.987
5.5	.715	-	-	-	.722	-	-	-	.727	.733	.737	.742	.812	.852	.956	.992
6.0	.741	-	-	-	.746	-	-	-	.750	.753	.757	.760	.822	.859	.960	.995
6.5	.767	-	-	-	.769	-	-	-	.771	.773	.774	.776	.830	.865	.962	-
7.0	.792	-	-	-	.792	-	-	-	.791	.791	.791	.792	.837	.870	.964	1.000
7.5	.816	-	-	-	.812	-	-	-	.810	.808	.806	.805	.844	.874	.965	-
8.0	.840	-	-	-	.832	-	-	-	.827	.824	.821	.817	.849	.877	.966	-
9.0	.885	-	-	-	.872	-	-	-	.861	.853	.847	.840	.858	.882	.967	-
10.0	.929	.922	.916	.911	.906	.901	.897	.893	.890	.880	.869	.860	.864	.886	.968	1.000
11.0	.970	.959	.953	.946	.939	.933	.927	.921	.917	.901	.888	.878	.870	.889	.968	-
12.0	1.010	.998	.988	.979	.970	.962	.955	.948	.942	.922	.906	.893	.873	-	-	-
13.0	1.049	1.034	1.022	1.009	.999	.990	.980	.973	.965	.941	.922	.907	.875	-	-	-
14.0	1.085	1.068	1.053	1.039	1.027	1.016	1.005	.996	.987	.958	.937	.921	.877	-	-	-
15.0	1.121	1.102	1.085	1.068	1.053	1.040	1.028	1.017	1.007	.975	.950	.932	.879	.893	-	-
16.0	1.156	1.133	1.112	1.094	1.077	1.063	1.049	1.037	1.026	.990	.963	.942	.881	-	-	-
18.0	1.223	1.193	1.167	1.144	1.123	1.105	1.088	1.073	1.060	1.016	.984	.960	.885	-	-	-
20.0	1.286	1.249	1.217	1.189	1.164	1.143	1.123	1.105	1.089	1.039	1.003	.975	.887	.894	-	1.000
22.0	1.347	1.302	1.264	1.231	1.202	1.177	1.154	1.134	1.116	1.059	1.018	.987	.889	-	-	-
24.0	1.404	1.352	1.308	1.269	1.237	1.208	1.182	1.160	1.140	1.077	1.032	.997	.891	-	-	-
26.0	1.460	1.399	1.348	1.305	1.268	1.236	1.208	1.183	1.161	1.092	1.043	1.005	.893	-	-	-
28.0	1.515	1.444	1.387	1.339	1.298	1.262	1.231	1.204	1.180	1.106	1.053	1.013	.894	-	-	-
30.0	1.565	1.487	1.423	1.370	1.325	1.286	1.253	1.224	1.198	1.118	1.061	1.019	.895	.895	-	1.000
32.0	1.617	1.528	1.458	1.399	1.351	1.309	1.273	1.241	1.214	-	-	-	-	-	-	-
34.0	1.665	1.568	1.490	1.427	1.374	1.330	1.291	1.258	1.228	-	-	-	-	-	-	-
36.0	1.712	1.605	1.521	1.453	1.397	1.349	1.308	1.273	1.242	-	-	-	-	-	-	-
38.0	1.757	1.641	1.551	1.478	1.418	1.367	1.324	1.287	1.254	-	-	-	-	-	-	-
40.0	1.801	1.676	1.579	1.501	1.437	1.384	1.339	1.300	1.266	-	-	-	-	-	-	1.000
45.0	1.908	1.757	1.643	1.554	1.481	1.422	1.372	1.328	1.292	-	-	-	-	-	-	-
50.0	2.010	1.833	1.702	1.601	1.520	1.455	1.400	1.353	1.313	-	-	-	-	-	-	1.000
55.0	2.107	1.902	1.756	1.644	1.555	1.483	1.425	1.375	1.332	-	-	-	-	-	-	-
60.0	2.199	1.967	1.803	1.680	1.585	1.508	1.445	1.392	1.347	-	-	-	-	-	-	1.000

Table VIII Tabulation of Data for N_{tu} vs. Maximum Slope with the Conduction Parameter as the third Variable.

APPENDIX A.

DATA REDUCTION RELATIONS

The following summary of some of the data reduction relations is given to clarify some of the definitions of the geometrical parameters, to show how they influence the deduced results and to facilitate an understand as to the exact procedure required to produce from raw data a point on the j vs N_R and f vs N_R curves.

The three most significant geometric parameters that afford a means of comparison between matrices are so defined that there exists a unique relation between them. Independent measurement of any two establishes the third or serves as a check on its independent measurement. The three primary surface geometry parameters of a matrix are:

1) HYDRAULIC DIAMETER:

$$4r_H = 4\frac{Ac}{A} L \tag{A-1}$$

2) POROSITY: Matrix Flow

$$p = \frac{\text{Void Volume}}{\text{Total Volume}} = \frac{A_c L}{A_{fr} L} = \frac{A_c}{A_{fr}} \tag{A-2}$$

3) AREA COMPACTNESS: Total Heat Transfer Surface Area

$$\beta = \frac{\text{Total Heat Transfer Surface Area}}{\text{Total Volume}} = \frac{A}{A_{fr} L} \tag{A-3}$$

NOTE: If equation (A-2) is divided by (A-3) the unique relation mentioned previously is formed.

$$r_H = p/\beta \tag{A-4}$$

MAXIMUM SLOPE:

As previously discussed, through the work of Locke, Mondt, Crestwick

and Howard, it has been established that the maximum slope of a generalized heating or cooling curve is a unique function of N_{tu} and λ, the conduction parameter,

$$\left[\frac{d\left(\frac{t_{f2} - t_i}{t_{f1} - t_i}\right)}{d(\tau / N_{tu})}\right]_{max} = f(N_{tu}, \lambda)$$

where

τ = generalized time variable

$$\tau = \frac{h A}{W_s c_s}\Theta$$

t_i = initial matrix temp.

t_{f1} = air temp. upstream

and $N_{tu} = \frac{h A}{\dot{m} c_p}$

t_{f2} = air temp. downstream

therefore:

$$\tau / N_{tu} = \dot{m} c_p / W_s c_s \Theta$$

and $$d(\tau / N_{tu}) = \dot{m} c_p / W_s c_s \, (d\Theta) \quad \text{.....(A-5)}$$

also:

$$\frac{t_{f2} - t_i}{t_{f1} - t_i} = \frac{t_{f2} - t_{f1}}{t_{f1} - t_i} + 1$$

and:

$$d\left(\frac{t_{f2} - t_i}{t_{f1} - t_i}\right) = \frac{1}{t_{f1} - t_i} \, d(t_{f2} - t_{f1}) \quad \text{..... (A-6)}$$

combining (A-5) and (A-6)

$$\left[\frac{d\left(\frac{t_{f2} - t_i}{t_{f1} - t_i}\right)}{d(\tau / N_{tu})}\right]_{max} = \frac{W_s c_s}{\dot{m} c_p} \cdot \frac{1}{t_{f1} - t_i} \, d\left(\frac{t_{f2} - t_{f1}}{d\Theta}\right) \quad \text{.....(A-7)}$$

The matrix is heated to a uniform temperature, t_i. The heat source is secured and the difference between downstream and upstream temperatures ($t_{f2} - t_{f1}$) is recorded vs. time. The maximum rate of change of this difference with time may be determined from the record.

From Figure 17:

$$\left[\frac{d(t_{f2} - t_{f1})}{d\theta} \right]_{max} = \frac{y}{x}$$

$$\frac{x}{\text{Chart speed}} = d\theta \quad \text{sec}$$

$$y = d(t_{f2} - t_{f1}) \quad \text{inches}$$

$$M = (t_{f1} - t_i) \quad \text{inches}$$

$$\frac{W_s c_s}{\dot{m} c_p} = \frac{\text{Matrix heat Capacitance}}{\text{Fluid heat Capacitance}} = \frac{\overline{C}_s}{C} \quad \frac{\text{BTU/°F}}{\text{BTU/°F sec}}$$

Finally, Equation (A-7) becomes:

$$\left[\frac{d\left(\frac{t_{f2} - t_i}{t_{f1} - t_i} \right)}{d\left(\tau / N_{tu} \right)} \right]_{max} = \frac{\overline{C}_s}{C} \cdot \frac{1}{M} \cdot \frac{y}{x} \cdot \text{Chart speed}$$

With this value of the maximum slope and a calculated value of λ, Howard's curves or tables may be entered to obtain a value of N_{tu}.

MASS FLOW RATE:

The mass flow rate is calculated as outlined in reference (7):

$$\dot{m} = 359 \; K \; D_o^2 \; FaY \sqrt{\Delta P_o \; \gamma}$$

where

K = flow coefficient, velocity of approach factor

Fa = thermal expansion factor

Y = expansion factor

D_o = orifice diameter, inches

γ = specific weight of fluid flowing at the orifice temperature lb/ft^3, corrected to existing atmospheric pressure

ΔP_o = Pressure drop across theorifice, inches H_2O

REYNOLD'S NUMBER:

By definition, the Reynolds number is

$$N_R = \frac{4r_H G}{\mu} \tag{A-8}$$

Where G is the mass flow velocity based on the flow mean cross-sectional area, A_c.

$$G = \frac{\dot{m}}{A_c} = \frac{\dot{m}}{p\, A_{fr}} \tag{A-9}$$

Note, if (A-9) is substituted into (A-8)

$$N_R = \frac{4\dot{m}}{\mu A_{fr}} \left(\frac{r_H}{\rho} \right) \tag{A-10}$$

but from (A-4) $r_H/\rho = \frac{1}{\beta}$ $\therefore$ $N_R = \frac{4\dot{m}}{\mu A_{fr}} \left(\frac{1}{\beta} \right)$ (A-11)

Therefore, for a given range of mass flows, the Reynolds number range for a given matrix is proportional to the inverse of its compactness.

$$N_R \propto 1/\beta$$

For ease of calculation, recall from (A-3) $\beta = \frac{A}{A_{fr} L}$

substituting into (A-11) yields

$$N_R = \frac{4L\dot{m}}{A\mu} \qquad \text{(A-12)}$$

THE FANNING FRICTION FACTOR:

The following sketch describes the flow system to be considered.

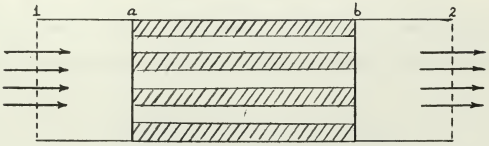

For gas flow heat exchanger application, the pressure changes from section 1 to a and from b to 2 are very small, relative to the total pressure, and therefore $v_a \simeq v_1$ and $v_b \simeq v_2$

The relation for the flow stream pressure drop calculation for most heat exchanger cores is (8):

$$\frac{\Delta P}{P_1} = \frac{G^2}{2g_c}\frac{v_1}{P_1}\left[\underbrace{(k_c + 1 - \rho^2)}_{\text{entrance effect}} + \underbrace{2\left(\frac{v_2}{v_1} - 1\right)}_{\text{flow acceleration}} + \underbrace{f\frac{A}{A_c}\frac{v_m}{v_1}}_{\text{core friction}} - \underbrace{(1 - \rho^2 - k_e)\frac{v_2}{v_1}}_{\text{exit effect}}\right] \qquad \text{(A-13)}$$

Solving (A-13) for f and recalling from (A-1) $A/A_c = L/r_H$ also $v = \frac{1}{\rho}$, we find:

$$f = \left[2g_c\rho_m\left(\frac{\Delta P}{G^2}\right) - \left(\frac{k_c}{\rho_1} + \frac{k_e}{\rho_2}\right)\rho_m - \rho_m\left(\frac{1}{\rho_2} - \frac{1}{\rho_1}\right)(1 + \rho^2)\right]\frac{r_H}{L} \qquad \text{(A-14)}$$

Now the perfect gas law may be applied since testing is done with air at moderate temperatures and pressures. Equation (A-14) becomes for the isothermal case:

$$f = \left[2g_c \rho_m \left(\frac{\Delta P}{G^2}\right) - \frac{P_1 + P_2}{2}\left(\frac{K_c}{P_1} + \frac{K_e}{P_2}\right) - \left(\frac{P_1 + P_2}{2}\right)\left(\frac{1}{P_2} - \frac{1}{P_1}\right)\left(1 + \rho^2\right) \right] \frac{r_H}{L} \qquad \text{(A-15)}$$

where $\frac{1}{\rho} = \frac{RT}{P}$ $\rho_m = \frac{\rho_1 + \rho_2}{2}$ and $T_1 = T_2$

The first term is by far the largest contributor to the friction factor for small pressure differentials, therefore making the approximations

$$\frac{P_1 + P_2}{2} = P_m \approx P_1 \approx P_2$$

Equation(A-15) becomes

$$f = \left[2g_c \rho_m \left(\frac{\Delta P}{G^2}\right) - \left(K_c + k_e\right) + \frac{\Delta P}{P_m}\left(1 + \rho^2\right) \right] \frac{r_H}{L} \qquad \text{(A-16)}$$

where: Kc = entrance coefficient

Ke = exit coefficient

whose values are determined from appropriate curves in Chapter IV, reference (8).

This is the equation used to determine the friction factor as presented in this thesis.

If a further assumption is made such that

$$f \approx 2g_c \rho_m \frac{\Delta P}{G^2} \frac{r_H}{L} \qquad \text{(A-17)}$$

and equations (A-4) and (A-9) are substituted, Equation (A-17) becomes:

$$f \approx \frac{2g_c \rho_m \Delta P}{\dot{m}^2}\left(\frac{A_{fr}}{L}^2\right)\frac{\rho^3}{\beta} \qquad \text{(A-18)}$$

Therefore, for a given matrix the friction factor is directly proportional to the cube of the porosity and indirectly proportional to the compactness.

$$f \approx \rho^3/\beta \tag{A-19}$$

COLBURN j FACTOR:

We have λ and maximum slope with which we get N_{tu} from Table VIII or Figure 18 taken from reference (5).

The j factor is defined as:

$$j = N_{ST} N_{PR}^{2/3} = \frac{h}{G c_p} N_{PR}^{2/3} \tag{A-20}$$

substituting (A-9) for G and multiplying by A/A

$$j = \frac{hA}{\dot{m} c_p} \frac{Ac}{A} N_{PR}^{2/3} \tag{A-21}$$

by definition:

$$N_{tu} = \frac{hA}{\dot{m} c_p}$$

Therefore:

$$j = N_{tu} \frac{Ac}{A} N_{PR}^{2/3} \tag{A-22}$$

Note, from (A-1) $Ac/A = r_H/L$, substituting ρ/β for r_H from (A-4) gives:

$$j = N_{tu} N_{PR}^{2/3} \frac{1}{L} \rho/\beta \tag{A-23}$$

which leads to the relation that for a given matrix, j is directly proportional to the porosity and inversely proportional to the compactness.

$$j \propto \rho/\beta$$

HEAT TRANSFER POWER AND FLOW FRICTION POWER:

The heat transfer power per unit area per degree temperature difference is derived as follows:

$$j = N_{ST} N_{PR}^{2/3}$$

$$N_{ST} = \frac{N_{Nu}}{N_R N_{PR}} = \frac{hD_H}{k} \cdot \frac{k}{c_p \mu} \cdot \frac{1}{N_R}$$

$$j = \frac{hD_H}{c_p \mu} \cdot \frac{1}{N_R} \cdot N_{PR}^{2/3}$$

Solving for h:

$$h = \frac{c_p \mu}{N_{PR}^{2/3}} \cdot \frac{1}{D_H} \cdot N_R \, j$$

Now if c_p, μ and N_{PR} are evaluated at standard properties which by convention are taken as those for dry air at 500°F and one atmosphere;

$c_p = 0.2477$ BTU/lb °F

$\mu = 0.0678$ lb/hr ft

$\rho = 0.0413$ lb/ft^3

$N_{PR} = 0.671$

Thus, the heat transfer power per unit area per degree temperature difference evaluated at the above standard conditions, h_{STD}, becomes

$$h_{STD} = .02195 \left(\frac{1}{4r_H} \right) (N_R \, j) \qquad \text{BTU/hr ft}^2\text{°F}$$

The flow friction power per unit area is derived as follows:

$$f \approx \frac{2 g_c \rho_m \Delta P \left(\frac{r_H}{L} \right)}{G^2}$$

$$\Delta P \left(\frac{r_H}{L} \right) = \frac{G^2 f}{2 g_c \rho_m}$$

$$E = \Delta P\left(\frac{r_H}{L}\right) V\left(\frac{1}{550}\right) = f\left[\frac{1}{2g_c}\left(\frac{1}{4r_H}\right)^3\left(\frac{\mu^3}{\rho^2}\right)\left(\frac{\rho V D_H}{\mu}\right)^3\right]$$

where $G = \rho V$

$$E = f\left[\frac{1}{2g_c}\left(\frac{1}{4r_H}\right)^3\left(\frac{\mu^3}{\rho^3}\right) N_R{}^3\right]$$

Now if μ and ρ are evaluated at standard properties (previously defined) the flow friction power per unit area evaluated at the above standard conditions, E_{STD}, becomes:

$$E_{STD} = 1.11 \times 10^{-7} \left(\frac{1}{4r_H}\right)^3 \left(\frac{N_R}{1000}\right)^3 f \quad \left[hp/ft^2\right]$$

Figure 16 provides a comparison of the 20° skew and the "parallel plate" matrices from a heat transfer power vs. friction power point of view (h_{STD} vs. E_{STD}). For comparison purposes the surface geometries have been adjusted to a common hydraulic diameter of $4r_H = 2 \times 10^{-3}$ ft.

APPENDIX B.

DESCRIPTION OF EQUIPMENT

To obtain heat transfer data, a transient technique was employed. Briefly, this method consists of heating the test matrix, to a uniform temperature and then subjecting the matrix to a step change in fluid flow temperature. The fluid temperature downstream of the matrix is recorded versus time.

Friction factor was calculated from pressure drop data obtained from static pressure taps located in the test section immediately upstream and downstream of the matrix.

The equipment necessary to complete the experiment falls into one of the following systems.

1) Fluid source
2) Flow metering system
3) Temperature measuring system
4) Pressure measuring system
5) Fluid heater
6) Matrix holder & test section casing

FLUID SOURCE:

The working fluid was, of course, air. Air was provided to the apparatus by placing the entire rig on the inlet to a 100cfm, 6 stage centrifugal air compressor. The compressor requires an operating voltage of 120^{V} at 90amp.

FLOW METERING SYSTEM: (See Figure 1)

The flow metering system consists of an orifice in a 3.08" inside diameter aluminum tube. The orifice section was constructed in accordance with the ASME specifications of reference (7) for standard D and D/2 pressure taps. A large flow range was obtained by means of 7 orifice

plates of throat diameter 2.310, 1.971, 1.232, 1.540, .462 and .308 inches, respectively. Accurate control of the pressure drop across the orifice was maintained by a large sliding valve downstream of the apparatus on the inlet to the compressor and another sliding valve on the discharge side of the compressor. There is an additional valve on the inlet side of the compressor that is fully open or fully closed. It is normally opened at flow rates less than 150 lb/hr to prevent stalling the compressor.

TEMPERATURE MEASURING SYSTEM: (See Figure 1)

Without exception, all temperatures were measured with iron-constantan thermocouples. A single thermocouple measured the orifice temperature (T_o) just upstream of the orifice at the inlet to the apparatus. This temperature was read in millivolts on a RUBICON CO. portable precision potentiometer, converted to temperature and recorded for each run. Measuring T_1 is a group of 5 thermocouples in series, bound together and insulated from each other by teflon tape and inserted in a 1/8" diameter aluminum tube. The tube was placed in the air stream with a small window cut in it facing upstream. At this point ambient air temperature was measured. T_2 and T_4 are 5 wire thermocouple grids permanently mounted in the test section cabinet. Their wires are connected in series to magnify the thermocouple output voltage. T_3 is a movable 5 wire thermocouple grid located in the matrix holder and is placed adjacent to and downstream of the matrix, it's wires are also in series. It's position is apparent in Figure 21. The thermocouples arranged in this manner provided flexibility and complete coverage of desired points of interest. If the thermocouple output voltages from T_2 and T_1 are bucked against each other,

the temperature measuring system response curves may be generated on a Leeds & Northrup "Speedomax" temperature recorder. T_2 vs T_4 gives the indication of temperature uniformity across the matrix and T_1 vs T_3 records the rate of change of the difference between upstream and downstream temperatures with time. It is this record that provides the primary data for the evaluation of heat transfer data. The precise relation of this record to the Colburn j factor is explained in Appendix A. The record is made on a Leeds and Northrup "Speedomax" Temperature Recorder. The recorder has variable chart speeds, which permits maintenance of acceptable cooling curves with regard to slope determination. The Speedomax also has a range of 0-20 mv. For this experiment, the recorder is precalibrated on a 3 mv. scale.

There is one addition thermocouple grid that is not used in the experiment, but was used in checking out the apparatus. This grid would take the place of T_3 and its purpose was to determine the temperature distribution across the cross section in both the vertical and horizontal directions. It was placed in a special holder that also held a velocity probe (See Figure 22) and was lined with balsa wood to provide a smooth and continuous internal flow passage.

PRESSURE MEASURING SYSTEM: (See Figure 1)

Pressure taps are located upstream and downstream of the orifice and upstream and downstream of the matrix. Each tap is connected by Saran tubing to an appropriate manometer or draft gage. The following instruments were used:

1) Type "C" micromanometer, E. Vernon Hill & Co. 0-1.25"
2) Ellison Differential Direct Draft Gage, 0-6", 0-8"
3) Ellison Inclined Draft Gage, 0-6"
4) Meriam Instrument Co. 0-60".

Any one or combination of these instruments can be used to measure the differential pressures of the orifice and the matrix. Frequent cross checks were made to ensure reliable operation.

FLUID HEATER SYSTEM: (See Figure 1)

The air heater section consists of 28 nichrome .0031" diameter wire heaters. The heater system is designed to heat 1000 pounds of air per hour, 20°F above ambient temperature. Nichrome was chosen because of its high resistivity, low thermal conductivity and low specific heat.

The nichrome wire is wound on a bakelite frame, two heaters to a frame. The wires are 1/32" apart and there are 50 and 52 wires respectively, to each heater on a frame. The heaters on each frame are connected in parallel and then connected through a switch, to a variable voltage bus. There are two frames to a plastic holder, as shown in Figures 23 and 24. In these figures, the heater frame and its electrical connections can be clearly seen.

A schematic wiring diagram for one frame is shown below. All 14 frames are wired in this manner, putting all 28 heaters in parallel with the capability of switching on or off two at a time.

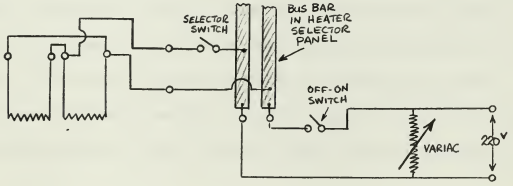

The 28 heaters arranged in this way, provide a variety of flexibility. The number of heaters in use, should decrease as the flow rate decreases. Voltage variation can be obtained by a GENERAL RADIO COMPANY "VARIAC", 0-240^{v}, 8a, 50-60 cycles. It is recommended that a voltage of 220^{v} or in this vicinity, be maintained, at all flow rates, and the number of heaters used, decreased until the number of heaters is four. At this point, the voltage should be decreased, as necessary, to obtain a 20° temperature rise, the number of heaters remaining constant. A note of caution: Do not energize a heater, unless the air is flowing, otherwise, the wires will sag due to thermal expansion and short circuiting will occur.

MATRIX HOLDER AND TEST SECTION:

The matrix holder and test section casing are made from polyethylene plastic. This material was chosen because of its low heat capacity.

The test section casing holds thermocouples T_2 and T_4 permanently mounted upstream and downstream respectively. It also contains the upstream and downstream static pressure taps used in determining the friction factor. The parts making up the casing were machined to close tolerances, to ensure a tight fitting matrix holder, and a minimum of air leaks.

The parts comprising the matrix holder, as implied above, were machined to close tolerances to ensure a tight fit. Great care was taken to ensure smooth alighment of the flow channel through the heaters and the test section. The size of the matrix holder was arbitrarily chosen. The flow channel dictated the width, and the length is such that matrices of various flow lengths, up to 3", may be tested. The flow channel is 3-3/16" x 3-3/16".

The matrix holder has one special provision and that is for the movable

thermocouple T_3. A small hole is drilled in the front, and the wires are led through. The matrices are placed in the holder and held in place by bits of Styrofoam plastic cut to the size necessary to hold the matrix square in the flow channel.

That completes a description of the various systems involved in the apparatus, but there is one other item that bears mentioning. Just upstream of the heater section, is a section provided for screens to straighten the velocity profile. Provisions were made for 1 to 4 screens. One 60 mesh stainless steel screen was found to be sufficient, to straighten the flow at the flow rates used (40-1000 lb/hr.)

APPENDIX C

CALCULATION OF GEOMETRIC CONSTANTS
FOR PERFORATED MATERIAL

As demonstrated in Appendix A, the surface geometry has a strong influence on the heat transfer and friction factor curves. Specifically, the effects of p and β were examined.

In using perforated materials, the presence of the slots, require modification of these two parameters. It is the intent of this Appendix, to demonstrate the calculation procedure utilized to determine the geometric parameters, on which the graphical and tabular results for the matrices constructed from perforated material are based.

The material used in the perforated plate matrices, was a pure nickel, type 160/40TV, slotted opening plate material, .0022 inches thick. This material is a product of Perforated Products, Inc.

The basic geometry of the plate is:

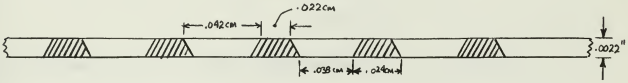

Using the average between the top and bottom of the tapered slots, consider an average slot pattern as:

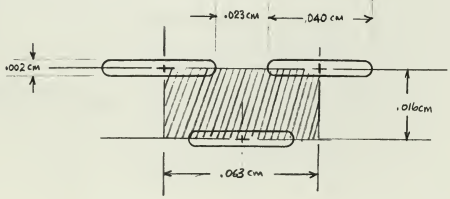

CROSS HATCHED AREA A_{ch} = (.063) (.016) = .001008 cm^2

AREA OF SLOT IN A_{ch} = (.040)(.0020) = .00008 cm^2

Now define γ = $\frac{A_{slot}}{A_{ch}}$ = AREA REDUCTION DUE TO SLOTS

$$\gamma = \frac{.00008}{.001008} = 7.93\%$$

Therefore, plate Porosity (p_s) = (1 - γ) = .9207

Now define δ = $\frac{\text{CROSS SECTION AREA OF SLOTS}}{\text{CROSS SECTION AREA}}$ = CONDUCTION AREA REDUCTION DUE TO SLOTS

$$\delta = \frac{(.040)(.0022)}{(.063)(.0022)} = 63.5\%$$

The following calculations are for the 20° skew perforated plate matrix:

DIMENSIONS OF PLATE: 4.285" x 1.98" x .0022"
NUMBER OF PLATES: 142
DIMENSIONS OF MATRIX: 3.255" x 3.248" x 1.98"
WEIGHT OF MATRIX: 275.5735 grams
MATERIAL CONSTANTS; ρ_s = 555 lb/ft^3

k_s = 38.7 $BTU/hr°F\ ft$

c_s = .1065 $BTU/lb°F$

PLANE SURFACE AREA = $\frac{(142)(4.285)(1.98)(2)}{144}$ = 16.733 ft^2

TOTAL HEAT TRANSFER AREA (A) = PLANE SURFACE AREA - AREA OF SLOTS

= (1- γ) SURFACE AREA

= (.9207)(16.733)

$$\boxed{A = 15.41\ ft^2}$$

FRONTAL AREA (A_{fR}) = 3.255 x 3.248 = 10.572 in^2

$$\boxed{A_{fr} = .0734\ ft^2}$$

FREE FLOW AREA = FRONTAL AREA - CROSS SECTIONAL AREA OF METAL

$= 10.572\ in^2 - 4.285 \times .0022 \times 142 = 9.233\ in^2$

$$\boxed{A_c = .06416\ ft^2}$$

CONDUCTION AREA (A_s) $= (142)(4.285)(.0022)(1-\delta)$

$= (142)(4.285)(.0022)(.375) = .50198\ in^2$

$$\boxed{A_s = .003486\ ft^2}$$

MAXTIX VOLUME (V_m) = 3.255" x 3.248" x 1.98" = $20.933\ in^3$

MATERIAL VOLUME (V_s) = 142x4.285"x1.98"x.0022" = $2.650\ in^3$

WEIGHT OF MATERIAL (W_s) = 275.5735 gms./453.6 gm/1b = .6075 lb.

MATERIAL VOLUME ($\overline{V_s}$) = W_s/ρ_s = .6075 1b/555 1b/ft^3 = $.001095\ ft^3$

The porosity of a matrix has been defined as:

$$p = \frac{\text{MATRIX FLOW VOID VOLUME}}{\text{MATRIX VOLUME}} = \frac{V_m - V_s}{Vm} = 1 - \frac{Vs}{V_m}$$

$$p = 1 - \frac{.001534}{.01211} = \boxed{.8733}$$

$$\overline{p} = 1 - \frac{\overline{V_s}}{V_m} = 1 - \frac{.001095}{.01211} = 1 - .09042 = .90958$$

The compactness of a matrix has been defined as

$$\beta = \frac{\text{TOTAL HEAT TRANSFER AREA}}{\text{MATRIY VOLUME}}$$

Here, we will redefine β to include the effect of area reduction:

$$\beta = \frac{(\text{PLANE SURFACE AREA})(1-\delta)}{\text{MATRIX VOLUME}}$$

For $\gamma = 0$

$$\beta = \frac{(16.733)(1)}{.01211} = 1381.75 \ ft^2/ft^3$$

For $\gamma = .0793$

$$\bar{\beta} = \frac{(16.733)(.9207)}{.01211} = \boxed{1272.18 \ ft^2/ft^3}$$

The hydraulic diameter is conventionally defined as:

$$D_H = 4 \ \frac{\text{FLOW CROSS SECTION AREA}}{\text{WETTED PERIMETER}}$$

Appendix A shows that hydraulic diameter can also be expressed as:

$$D_H = 4 \ P/\beta$$

To be consistent with the conventional definition, for the case of a perforated material, β is used vice $\bar{\beta}$, since the slots have no effect on the hydraulic diameter.

Finally then,

$$D_H = 4 \ \frac{.8733}{1381.75} = \boxed{.002528 \ ft}$$

APPENDIX D

SAMPLE CALCULATIONS

The following sample calculations are based on recorded data from Run #3 for 20° skew matrix constructed from perforated nickel sheets. This is chosen primarily because the basic geometric parameters are computed in Appendix C.

RECORDED DATA:

$D_o = 2.310"$ $\quad P_{atm} = 29.963$ in. Hg

$\Delta P_o = 2.61$ in. H_2O $\quad$ CHART SPEED = 4.0 in/sec

$\Delta P_m = 3.96$ in. H_2O $\quad W_m = .6075$ lb

$P_s = 4.69$ in. H_2O

$T_o = 68.0$ °F

MATERIAL CONSTANTS:

$c_s = .1065$ BTU/lb °F

$k_s = 38.7$ BTU/hr ft°F

PRECALCULATED GEOMETRIC PARAMETERS: (Re: Appendix C)

$A = 15.41$ ft^2 $\quad \rho = .8733$

$A_{fr} = .0734$ ft^2 $\quad \bar{\beta} = 1272.18$ ft^2/ft^3

$A_c = .06416$ ft^2 $\quad r_H = .000632$ ft

$\bar{A}_s = .003486$ ft^2

$L = 1.98$ inches ($\bar{}$ denotes corrected for slot effects)

DETERMINATION OF MASS FLOW: as outlined in Reference (7)

$$m = 359\ K\ D_o^2\ F_a\ Y\ \sqrt{\Delta P_o\ \gamma}$$

where: $Y \approx 1.0$ Fig. 40b Ref. (7)

$F_a \approx 1.0$ Fig. 38 Ref. (7)

$$\dot{m} = (359)(2.31)^2 \; K \sqrt{(2.61)\left(\frac{29.963}{29.92}\right)(.07522)}$$

$$\dot{m} = 849.40 \; K$$

assume $K = .749$ $\qquad \beta = d/D = \frac{2.31}{3.08} = .75$

Then $\dot{m} = (849.40)(.749) = 636.21$ lb/hr

Reynold's number for the pipe $N_{Rp} = \frac{4\dot{m}}{\pi D \mu}$

$$N_{Rp} = \frac{(4)(636.21)(12)}{(\pi)(3.08)(.04410)} = 7.35 \times 10^4$$

From Table 5, Ref. (7) $\beta = 0.75$, $N_R = 7.35 \times 10^4$, $K = .749$

Therefore $\boxed{\dot{m} = 636.21 \text{ lb/hr}}$

MATRIX REYNOLD'S NUMBERS

There are actually two Reynold's numbers to be calculated for the matrix. One is for isothermal flow and is associated with the friction factor, the other is associated with heat transfer. They differ only in the temperature at which the absolute viscosity μ is evaluated. μ_f (friction) is evaluated at ambient temperature (T_o). μ_H (heat transfer) is evaluated at T_o + 10°F (an estimate of the average bulk fluid temperature).

$$N_R)_f = \frac{4L\dot{m}}{A\mu_f} = \frac{(4)\left(\frac{1.98}{12}\right) \text{ ft}(636.21 \text{ lb/hr})}{(15.41 \text{ft}^2)(.04405 \text{ lb/ft hr})} = 618.58$$

$$N_R)_H = \frac{4L\dot{m}}{A\mu_H} = N_R)_f \frac{\mu_f}{\mu_H} = (618.58)\left(\frac{.04405}{.04470}\right) = 609.58$$

CONDUCTION PARAMETER

$$\lambda = \frac{k_s A_s}{L \dot{m} C_p} = \frac{(38.7)(.003486)(12)}{(1.98)(636.21)(.24)} = \boxed{.00536}$$

MAXIMUM SLOPE

From Figure 26 the slope of the cooling curve was determined as described in Appendix A. The slopes of three curves were determined and the average of the three was used in the calculations.

$$\text{MAXIMUM SLOPE} = \frac{\overline{C}_s}{C}\left(\frac{dT}{d\theta}\right)_{max} = \frac{\overline{C}_s}{C} \times \text{SLOPE xCHART SPEED}$$

$$\overline{C}_s = W_s c_s = (.6075\ \text{lb})(.1065\ ^{BTU}/_{lb°F}) = .06470\ ^{BTU}/_{°F}$$

$$C = \dot{m}\, c_p = (636.21\ ^{lb}/_{hr})(.24\ ^{BTU}/_{lb°F})\ \frac{hr}{3600\ sec}$$

$$= .04241\ ^{BTU}/_{sec\ °F}$$

SLOPE = .16014 in^{-1} (See Figure 26)

Finally:

$$\text{MAXIMUM SLOPE} = \frac{(.06470)}{(.04241)}\ (.10775)\ 4) = \boxed{.65745}$$

COLBURN j FACTOR

With λ and MAXIMUM SLOPE enter Table VIII and find $N_{tu} = 4.40$. Linear extrapolation will give desired accuracy.

Now,

$$j = N_{tu}\ \frac{A_c}{A}\ N_{PR}^{2/3} \quad \text{from Appendix A, Eq. (A-22)}$$

therefore, $j = \frac{.06416}{15.41}\ (.796)(4.40) = \boxed{.01458}$

FANNING FRICTION FACTOR

As derived in Appendix A Equation (A-16) the friction factor is:

$$f = \left[2g_c \rho_m \left(\frac{\Delta P}{G^2}\right) - \left(K_c - K_e\right) - \frac{\Delta P_m}{P_{mean}}\left(1 + P^2\right)\right]\frac{r_H}{L}$$

$\Delta P_m = 3.96$ in H_2O x 5.204 $\frac{psf}{in\ H_2O}$ = 20.61 psf = .1431 psi

$$\Delta P_s = 4.69 \text{ in } H_2O \times 5.204 \frac{\text{psf}}{\text{in } H_2O} = 24.41 \text{ psf} = .1695 \text{ psi}$$

$$P_{atm} = 29.963 \text{ in } H_g \times .4912 \frac{\text{psi}}{\text{in } H_f} = 14.7178 \text{ psi}$$

$$P_1 = P_{atm} - P_s = 14.7178 - .1695 = 14.5483 \text{ psi}$$

$$P_2 = P_1 - P_m = 14.5483 - .1431 = 14.4052 \text{ psi}$$

$$P_{mean} = \frac{P_1 + P_2}{2} = 14.4768 \text{ psi}$$

$$\rho_{mean} = \frac{(P_{mean})(144)}{R\,T_m} = \frac{(14.477)(144)}{(53.3)(528)} = .07407 \ ^{lb}/_{ft^3}$$

$$G = \frac{\dot{m}}{A_c} = \frac{636.21 \text{ lb/hr}}{.06416 \text{ ft}^2} = 9915.9 \text{ lb/hr ft}^2 = 2.754 \ ^{lb}/_{sec\ ft^2}$$

$$r_{H/L} = \frac{.000632}{1.98/12} = .00383$$

$K_e = -.738$ $\quad K_c = .949$ from Chapter IV Reference (8)

$$(1 + p^2) = 1 + (.8733)^2 = 1.7626$$

$$2g_c \rho_{mean} \frac{\Delta P_m}{G^2} = \frac{(64.4)(.07407)(20.61)}{7.587} = 12.9579$$

$$\frac{\Delta P_m}{P_{mean}} (1+p^2) = \frac{.1431 \text{ psi}}{14.4768 \text{ psi}} (1.761) = .01742$$

$$f = (12.9579 - .01740 - .211)(.00383) = (12.7295)(.00383)$$

$$= \boxed{.04859}$$

All thermal properties (μ, N_{PR}, k_s, and c_s) were obtained from References (12) and (13). The temperature at which the properties were

evaluated was the ambient temperature with the exception of the absolute viscosity for heat transfer (μ_H).

APPENDIX E

A FORTRAN COMPUTER PROGRAM
FOR DATA REDUCTION

A short computer program was devised, Figure 27, so that from basic experimental data, the end result is:

1) Conduction parameter (λ)
2) Maximum slope
3) Reynold's number for heat transfer
4) Reynold's number for friction
5) Fanning friction factor

It was anticipated that this program along with a subroutine would ultimately produce N_{tu} and subsequently the Colburn j factor.

Time did not permit the adaption of Moreland's work (11) to a subroutine but the program is still useful. It's value when data for a single matrix is to be reduced is nebulous. However, the reduction of data for multiple matrices can be accomplished with a considerable savings of time.

The following is a list of inputs necessary in Fortran and English language along with the required dimensions:

CARD NO.			
30	XML	Matrix length	ft
	AS	Solid conduction area	ft^2
	RH	Hydraulic radius	ft
	POR	Porosity	-
	AFL	Flow cross section area	ft^2
	AHT	Matrix heat transfer area	ft^2
	WM	Matrix weight	lbs

CARD NO.			
40	EK	Exit flow coefficient	-
	CK	Entrance flow coefficient	-
	SK	Solid thermal conductivity	BTU/hr°F ft
	CM	Matrix material specific heat	BTU/lb°F
	N	Number of runs	-
10	DO	Diameter of orifice plate opening	inches
	DELPO	Pressure drop across orifice	inches H_2O
	GAM	Specific weight of fluid	lbs/ft^3
	ATMP	Atmospheric pressure	inches Hg
	COR	Orifice correction K	-
	UH	Fluid viscosity for heat transfer	lb/hr ft
	UFR	Fluid viscosity for friction	lb/hr ft
10+2	CS	Chart speed	sec/inch
	DELH	Pressure drop across matrix	inches H_2O
	HS	Static pressure matrix inlet	inches H_2O
	SLO	Slope of generalized cooling curve	$(inches)^{-1}$
	TEMPO	Orifice temperature	°F

The output of this program in Fortran and English language along with their dimensions is:

EMDOT	Mass flow rate ($\dot{m}$)	lb/hr
RNUMP	Reynold's number for the pipe	-
RNUMH	Reynold's number for heat transfer	-
CAPFL	Thermal capacitance of the fluid (C)	BTU/sec °F
CAPS	Thermal capacitance of the solid (C_s)	BTU/ °F
CONDPAR	Conduction parameter (λ)	-

SLOMAX	Maximum slope of generalized cooling curve	-
G	Mass flow velocity	lb/hr ft^2
RNUMFR	Reynold's number for friction	-
FFR	Fanning Friction factor	-

Reduction of data is not complete since j remains to be found. With SLOMAX and CONDPAR, enter Table VIII, and find N_{tu}. The Colburn j factor follows from equation (A-22), Appendix A.

The program is flexible in that an unlimited number of matrices may be reduced by changing the first card of the program appropriately. (L = the number of matrices to be reduced.)